Tellus SERIES A DYNAMIC METEOROLOGY AND OCEANOGRAPHY
PUBLISHED BY THE INTERNATIONAL METEOROLOGICAL INSTITUTE IN STOCKHOLM

Tropical cyclones in the GISS ModelE2

By SUZANA J. CAMARGO[1]*, ADAM H. SOBEL[1,2,3], ANTHONY D. DELGENIO[4], JEFFREY A. JONAS[4,5], MAXWELL KELLEY[4], YUN LU[6], DANIEL A. SHAEVITZ[2] and NAOMI HENDERSON[1], [1]*Lamont-Doherty Earth Observatory, Columbia University, Palisades, NY, USA*; [2]*Department of Applied Physics and Applied Mathematics, Columbia University, New York, NY, USA*; [3]*Department of Earth and Environmental Sciences, Columbia University, New York, NY, USA*; [4]*NASA Goddard Institute for Space Studies, New York, NY, USA*; [5]*Center for Climate System Research, Columbia University, New York, NY, USA*; [6]*Ningbo Meteorological Office, Ningbo City, Zhejiang, China*

(Manuscript received 2 March 2016; in final form 29 June 2016)

ABSTRACT

The authors describe the characteristics of tropical cyclone (TC) activity in the GISS general circulation ModelE2 with a horizontal resolution $1^\circ \times 1^\circ$. Four model simulations are analysed. In the first, the model is forced with sea surface temperature (SST) from the recent historical climatology. The other three have different idealised climate change simulations, namely (1) a uniform increase of SST by 2 degrees, (2) doubling of the CO_2 concentration and (3) a combination of the two. These simulations were performed as part of the US Climate Variability and Predictability Program Hurricane Working Group. Diagnostics of standard measures of TC activity are computed from the recent historical climatological SST simulation and compared with the same measures computed from observations. The changes in TC activity in the three idealised climate change simulations, by comparison with that in the historical climatological SST simulation, are also described. Similar to previous results in the literature, the changes in TC frequency in the simulation with a doubling CO_2 and an increase in SST are approximately the linear sum of the TC frequency in the other two simulations. However, in contrast with previous results, in these simulations the effects of CO_2 and SST on TC frequency oppose each other. Large-scale environmental variables associated with TC activity are then analysed for the present and future simulations. Model biases in the large-scale fields are identified through a comparison with ERA-Interim reanalysis. Changes in the environmental fields in the future climate simulations are shown and their association with changes in TC activity discussed.

Keywords: Hurricanes, global climate model, climate change

1. Introduction

As the spatial resolutions of climate models have increased in recent years, some climate models have been shown to simulate some characteristics of tropical cyclone (TC) activity well (e.g. Zhao et al., 2009; Camargo and Wing 2016). However, there is still a large spread in the quality of simulated TC activity from one climate model to another, as shown in Camargo (2013) for the phase 5 of the Coupled Model Intercomparison Project (CMIP5) models (Taylor et al., 2012). Although higher resolution generally improves the ability of a model to simulate TCs (Strachan et al., 2013; Manganello et al., 2014; Roberts et al., 2015), it is not sufficient; models of similar resolutions generate TCs with very disparate characteristics (Reed and Jablonowski, 2011; Shaevitz et al., 2014). Various other factors besides resolution can affect the quality of TC simulation in climate models, in particular the convection scheme (Vitart et al., 2001; Stan, 2012; Murakami et al., 2012a; Zhao et al., 2012), as well as the model dynamical core (Reed et al., 2015). Therefore, it is important to examine the ability of new climate models to simulate TC activity.

Here, we analyse the TC activity in the GISS general circulation ModelE2. A full description of this model is given in Schmidt et al. (2014), using the horizontal resolution that was used in the CMIP5 archive ($2^\circ \times 2.5^\circ$), while a description of the CMIP5 historical simulations of this model is given in Miller et al. (2014). Kim et al. (2012) examined the sensitivity of both the simulated Madden–Julian oscillation and TC activity to changes in the convection scheme in the GISS model at the same $2^\circ \times 2.5^\circ$ resolution, including the TC activity in that analysis.

*Corresponding author.
email: suzana@ldeo.columbia.edu

Citation: Tellus A 2016, **68**, 31494, http://dx.doi.org/10.3402/tellusa.v68.31494

Here, we consider the same model, but with a finer horizontal resolution ($1^\circ \times 1^\circ$) and focus on TC activity on the model and the environmental variables that are known to influence TC activity.

Due to the large impacts of TCs globally, it is important to understand well how TC activity will change in a warming climate. As part of the US Climate Variability and Predictability Program (CLIVAR) Hurricane Working Group (HWG), many modelling groups performed simulations using the same forcings, representing the recent historical climate as well as idealised representations of future climate change (Walsh et al., 2015). The simulations analysed here were performed as part of this multimodel ensemble. Shaevitz et al. (2014) present an overview of the performance of the entire ensemble for the simulations of recent historical climate and include the present climate simulation examined here in the GISS model as part of that. Here, we focus exclusively on the GISS model and analyse it in detail. We include the idealised climate change simulations and complement the analysis of TC activity with an analysis of large-scale environmental variables relevant to TC activity, neither of which was included in Shaevitz et al. (2014).

In Section 2, we give a short description of the ModelE2 simulations and the tracking algorithm used. In Section 3, the TC activity in ModelE2 is shown in the present climate. The changes in TC activity with climate change are discussed in Section 4. The large-scale environment is analysed in Section 5 and our conclusions are given in Section 6.

2. Model and data

2.1. GISS ModelE2

A detailed description of GISS ModelE2 appeared in Schmidt et al. (2014). Here, we just give a short summary of the model characteristics. The GISS climate model has had many versions, developing over the last 30 yr, with the model documented in various studies (e.g. Hansen et al., 1983, 2000; Schmidt et al., 2006). The latest model version, ModelE2, was developed for the CMIP5 experiments and used the opportunity to explore model forcings and feedbacks, assessing the impacts of multiple forcings and their dependence on model physics. The GISS ModelE2 CMIP5 simulations are discussed in Miller et al. (2014) (historical simulations) and Nazarenko et al. (2015) (future projections).

One of the main improvements of ModelE2 compared with the previous GISS model is the availability of interactive chemistry and aerosols (including dust). The updates and model performance of these chemistry simulations are described in Shindell et al. (2013), Voulgarakis et al. (2011) and Koch et al. (2011). Six GISS ModelE2 versions are included in the CMIP5 archive, with varying treatments of atmospheric composition, aerosol indirect effects and the ocean (Schmidt et al., 2014). Here, we consider the most basic version of the model, with non-interactive chemistry and tuned aerosol indirect effect, as described in Hansen et al. (2005). In our simulations, as per the specifications of the CLIVAR HWG, the GISS atmospheric model is forced with fixed sea surface temperature (SST) rather than being coupled to an interactive ocean. We also considered fixed values for ozone and aerosols based on the CMIP3 specifications (Meehl et al., 2007).

While the CMIP5 model description given in Schmidt et al. (2014) uses the typical horizontal resolution of $2^\circ \times 2.5^\circ$ on a Cartesian grid, in our simulations we used a version of the model with finer resolution, namely C90 (or approximately $1^\circ \times 1^\circ$) on a cubed sphere grid, which has not been described previously by the GISS modelling group. These cubed sphere grid versions of the model use the finite volume dynamical core as implemented by the Global Modelling and Assimilation Office (GMAO) at NASA Goddard Space Flight Center (GSFC) (Suarez and Takacs, 1995). The GISS ModelE2 with 1° horizontal resolution has the same physics as the 2.5° model. The GISS ModelE2 has 40 vertical layers and a model top at 0.1 hPa, which required modifications in the gravity wave drag scheme applied above 150 hPa (Rind et al., 1988), to only include effects of mountain waves and deformation waves (Schmidt et al., 2014). The radiation treatment of ModelE2 is as described in Schmidt et al. (2006) and Collins et al. (2006), with minor changes. The mass flux cumulus parameterisation is based on Del Genio and Yao (1993), and the stratiform cloud parameterisation on Del Genio et al. (1996).

2.2. Simulations

The model simulations analysed were performed as part of the US CLIVAR Working Group (HWG; www.usclivar.org/working-groups/hurricane). The HWG experiments were designed for a multimodel intercomparison of TC activity in different climate models. An overview of the US CLIVAR HWG is given in Walsh et al. (2015).

The HWG experiments are atmosphere-only simulations forced with fixed SST and CO_2 (Yoshimura and Sugi, 2005; Held and Zhao, 2011) in four different experiments: (1) a control simulation (called 'control') forced by climatological seasonally varying SSTs and sea ice concentration from the period 1985 to 2001 and 1992 atmospheric gas concentrations; (2) a plus 2K experiment (p2K), in which 2K is added uniformly to the climatological SSTs of the control experiment; (3) a doubled CO_2 (CO_2) experiment with twice the CO_2 concentration but the same SSTs as in the control experiment and (4) a combination of experiments p2K and CO_2, that is, with twice the CO_2 concentration and 2K added to the SSTs (p2KCO_2) of the control experiment. A summary of the experiments is given in Table 1.

Table 1. Model simulations analysed

Name	Abbreviation	SST type	CO_2	Length
Control	Control	Clim.	Fixed	20
Plus 2K	p2K	Clim. + 2K	Fixed	20
$2 \times CO_2$	CO_2	Clim.	$2 \times$	20
$+2K\ 2 \times CO_2$	$p2KCO_2$	Clim. + 2K	$2 \times$	20

The climatological (clim.) SST were obtained by averaging the observed monthly SST for the years 1985–2001. The fixed value (fixed) of CO_2 is from 1992. The lengths of the simulations are given in years.

Various aspects of the HWG multimodel TC intercomparison, for all models, or individual models or a subset of models have already been analysed and published, including Held and Zhao (2011), Elsner et al. (2013), Strazzo et al. (2013), Camargo et al. (2014), Horn et al. (2014), Mei et al. (2014), Patricola et al. (2014), Scoccimarro et al. (2014), Shaevitz et al. (2014), Villarini et al. (2014), Wang et al. (2014), Wehner et al. (2014), Daloz et al. (2015) and Wehner et al. (2015). Each of these papers had a different focus, either on a specific basin, for example, the Atlantic (Elsner et al., 2013; Strazzo et al., 2013; Mei et al., 2014; Patricola et al., 2014; Wang et al., 2014; Daloz et al., 2015) or on different aspects of the TC characteristics globally, such as the ability of the models to reproduce the current global climate TC climatology (Shaevitz et al., 2014), TC-associated precipitation (Scoccimarro et al., 2014; Villarini et al., 2014) or sensitivity to tracking algorithm (Horn et al., 2014). As mentioned above, our focus here is on only one of the HWG models, namely the GISS ModelE2 with $1^\circ \times 1^\circ$ resolution.

2.3. *Detection and tracking scheme*

To detect and track the TCs in the model simulations, we used the Camargo and Zebiak (2002) scheme, where it is described in detail. The Camargo–Zebiak scheme was originally developed for tracking TC-like vortices in low-resolution climate models for seasonal forecasting, based substantially on prior studies (Bengtsson et al., 1995; Vitart et al., 1997). This scheme has been used extensively in studies with global (e.g. Camargo et al., 2005; Walsh et al., 2010; Kim et al., 2012; Camargo 2013) and regional climate models (Landman et al., 2005; Camargo et al., 2007b), as well as operationally for seasonal TC forecasting (Camargo and Barnston, 2009; Schemm and Long, 2013).

The Camargo–Zebiak scheme uses model-dependent thresholds based on selecting the tails of the joint probability distributions of relevant 6-hourly model output variables: 850 hPa relative vorticity, 850–300 hPa anomalous integrated temperature and 10 m wind speeds. While in the original Camargo–Zebiak scheme these thresholds were basin dependent, here we use global thresholds. The thresholds are defined objectively, so there is no 'tuning'. These thresholds are defined based on the variances of the model variables – for example, in the case of the low-level vorticity, twice the standard deviation of the model vorticity distribution.

The following criteria are used to detect and track storms: (1) a local minimum in sea level pressure; (2) a local maximum in 850 hPa relative vorticity larger than or equal to the vorticity threshold (here, $3.4 \times 10^{-5}\ s^{-1}$); (3) a positive local temperature anomaly, greater than or equal to the standard deviation of the warm core temperature distribution (here, 0.9 °C); (4) a larger temperature anomaly at 300 hPa than at 850 hPa; (5) surface wind speed equal to or greater than the global average wind speed over water plus the standard deviation of the wind speed distribution (here, 9 m/s) and (6) higher mean wind speeds at 850 hPa than at 300 hPa.

The grid points in the model output that satisfy the criteria above are then connected into tracks if they are within a certain distance (here 5.5° of latitude or longitude) of each other. The tracks are compared with exclude repeated tracks and are required to last a minimum of 1.5 d. These tracks are subsequently extended forward and backwards in time by tracking a 850 hPa vorticity maximum, while the vorticity exceeds a more relaxed vorticity threshold, to achieve more realistic track lengths. It should be noticed that even imposing a warm core requirement on the storms, extratropical storms are not completely eliminated by our scheme – a common problem in tracking algorithms (Horn et al., 2014). In Camargo (2013), an additional constraint was imposed, by only considering storms forming in the tropics (30°S to 30°N), which was not applied here.

Monsoon depressions have very similar characteristics to weak TCs and can be tracked with the same algorithm, distinguished only by the storm intensity (Hurley and Boos, 2015). Therefore, it can be very difficult to distinguish them in cases of a model bias towards weak TCs, as is the case here. This issue seems to be particularly important in the North Indian Ocean. To estimate the potential role of the monsoon depressions in the model TC statistics, we compare the annual number of TCs in that basin, with the number of TCs during the North Indian TC season only (April–June, October–December) in our analysis.

Horn et al. (2014) examined the sensitivity of the HWG simulations to tracking schemes. They concluded that there is moderate agreement among different tracking methods, with some models and experiments showing better agreement than others, mainly due to duration, wind speed and latitude thresholds. The largest disagreements occur when the threshold from one tracking scheme is much higher than the other, with the first resulting in very few storms in the model, while the second leads to many more storms.

In the first case, when there are very few storms detected overall, the changes in storm frequency due to climate change are also small, and often not statistically significant, although statistically significant changes (such as increases in storm frequency) may be found when more generous thresholds are used.

2.4. Data

We compare the TC activity in the present day simulations with observations. The observed TC data in the eastern North Pacific, central North Pacific and North Atlantic are from the National Hurricane Center best-track data sets (Landsea and Franklin, 2013; downloaded in July 2015), and in the western North Pacific, North Indian Ocean and Southern Hemisphere from the Joint Typhoon Warning Center best-track data sets (Chu et al., 2002; JTWC, 2016). We consider statistics of the TC observations for the 20-yr period 1985–2004, which includes, but is slightly longer than, the 16 yr used to obtain the SST climatology (1985–2001). We choose the 20-yr period for the observed TC statistics because 20 yr is the duration of the model simulations.

To evaluate the model's simulation of large-scale environmental fields, we compare with the ERA-Interim reanalysis (Dee et al., 2011) averaged over the period 1985–2004. The monthly potential intensity (PI) was calculated using the formulation developed by Emanuel and co-authors (Emanuel, 1988, 1995; Bister and Emanuel, 1998, 2002a, b) using the monthly fields from the ERA-Interim reanalysis for the atmospheric fields and SST.[1]

The TC Genesis Index is a modified version of that described in Tippett et al. (2011). This index is derived from TC observations and climatological observations of environmental fields using Poisson regression. This technique has been used previously to obtain environmental indices describing the formation of TCs (Tippett et al., 2012), tornadoes (Tippett et al., 2014), hail (Allen et al., 2015a, b) and monsoon depressions (Ditchek et al., 2016). In our original version, TCGI is a function of the clipped absolute vorticity (described below), vertical wind shear, relative SST and column integrated relative humidity (Tippett et al., 2011). However, in Camargo et al. (2014), we showed using the Geophysics Fluid Dynamics Laboratory (GFDL) High-Resolution Atmospheric Model (HiRAM) that the optimal combination of predictors to analyse climate change simulations uses PI instead of relative SST and column saturation deficit instead of column relative humidity (Camargo et al., 2014). In the version of the TCGI used here, we trained the regression coefficients on the ERA-Interim reanalysis climatological fields, interpolated to a 2° grid. We then used the same coefficients to calculate the TCGI for the GISS model in all scenarios – that is, the index was not retrained on the GISS TC and environmental model fields. This allows us to see biases in the model environmental variables relevant to TC activity.

The saturation deficit is the difference between the column integrated water vapour and the same quantity at saturation, calculated as in Bretherton et al. (2004). While relative humidity tends to vary rather little as the climate warms (Sherwood et al., 2010; Wright et al., 2010), the saturation deficit increases systematically (Camargo et al., 2014). This increasing saturation deficit is believed on theoretical grounds (in addition to the empirical results of Camargo et al., 2014) to be relevant to the response of TC activity to climate change (Emanuel, 2010; Tang and Emanuel, 2012).

The clipped vorticity was defined in Tippett et al. (2011) and takes into account that the sensitivity of TC genesis on low-level absolute vorticity saturates after the vorticity exceeds a threshold (here 3.7×10^{-5} s^{-1}). Using a clipped vorticity leads to a better fit of the genesis index to observations.

3. Model TC activity in the present climate

In this section, we will discuss the main characteristics of the TC activity in the GISS model in the present climate. The tracks for TCs in 10 yr of the control simulation and observations are shown in Fig. 1. A few model biases stand out when comparing the two panels. The first is the low level of TC activity in the North Atlantic and eastern North Pacific. The second is that the region of TC activity in the North Pacific extends from eastern to western Pacific in the model with increasing numbers from east to west, while in observations there is a minimum in the central North Pacific. In the Indian Ocean, while the model is more active than observations in the Northern Hemisphere, the opposite occurs in the Southern Hemisphere. An analysis of the statistics of TC frequency gives us more detailed information on the differences between model and observations.

Figure 2 shows the characteristics of a GISS model TC: a maximum in relative vorticity, a minimum in sea level pressure, a maximum in the surface wind speed in the northeast quadrant of the storm and a hint of a minimum in the centre characterising the eye, and two precipitation maxima, one in the northeast quadrant and other (with smaller values) in southwest quadrant, similar to observed TC structures (see, e.g. Corbosiero et al. 2006). However, due to the horizontal resolution, the intensity of the storm is much lower than that of typical observed storms, and its

[1]The options considered in the PI code were: $C_k/C_d = 0.9$, pseudo-adiabatic ascent, dissipative heating allowed and a surface reduction factor of 0.8.

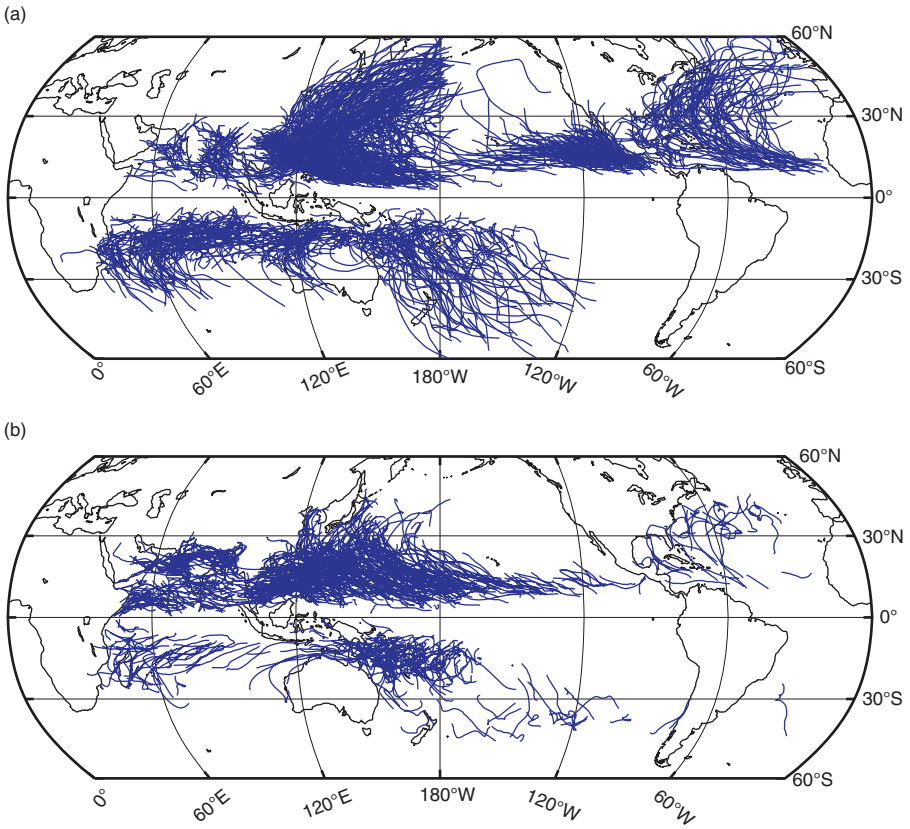

Fig. 1. Global tropical cyclone tracks in 10 yr of (a) observations (1992–2001) and (b) in the model control simulation.

size is larger than typical observed ones, similar to what is found in other lower resolution climate models (Bengtsson et al., 1995; Camargo and Wing, 2016).

In Table 2, the mean, percentage and standard deviation of the number of TCs globally, per basin and per hemisphere are given for the control simulation, the ensemble mean of the interannual simulations and observations. The mean global number of TCs in the GISS model (73.9) in the control simulation is close to the observed mean (81.8) (also shown in Fig. 3). In observations, the Northern Hemisphere has a much higher percentage of TCs (69.7 %) than in the Southern Hemisphere (30.3 %); in the GISS model control simulation, the contribution of the two hemispheres is quite similar to the observed, with only a slightly higher percentage in the Northern Hemisphere (74.4 %).

The occurrence of TC-like storms in the North Indian Ocean during the monsoon season is a common problem in global models, especially in low-resolution models (Camargo et al., 2005), as well as in some high-resolution models (Shaevitz et al., 2014). The occurrence of these North Indian storms during the monsoon season could be due to the inability of the tracking scheme and/or the model to differentiate between monsoon depressions and weak TCs. To estimate the influence of the off-season North Indian Ocean TCs (or potential monsoon depressions) in model TCs statistics, in Table 1 we also present the North Indian totals during the April–June and October–December only (North Indian*), excluding the possible contamination of the monsoon depressions during the monsoon season (July–September). The modified statistics (denoted by asterisk) for the Northern Hemisphere and Globe when considering only the TCs for the North Indian TC season (North Indian*) are also shown. There is a significant decrease in the importance of the North Indian Ocean for the global statistics when this is done (from 16.6 to 8.6 %), while the changes for the whole Northern Hemisphere and the globe are much smaller.

Figure 3 shows the distribution of the global number of TCs (NTC) in the model and observations, with the box denoting the interquartile ranges of each distribution, the red line the median and the red asterisk the median. In the control simulation, the GISS model has fewer TCs globally than observations do. The NTCs in the three future simulations will be discussed in Section 4.

A common measure of TC activity is the accumulated cyclone energy (ACE), which is defined as the sum of the squares of the maximum wind speed over all 6-h intervals

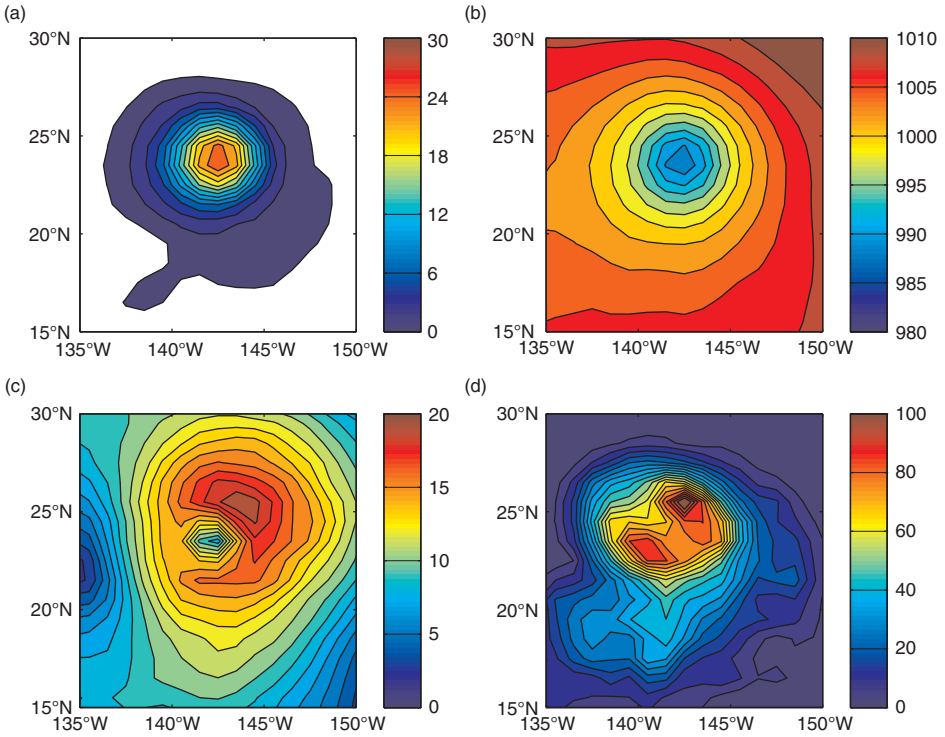

Fig. 2. Structure of a typical GISS model tropical cyclone (a) relative vorticity at 850 hPa $\times$ in s^{-1}, (b) sea level pressure (hPa), (c) daily mean surface wind speed (m/s) and (d) daily mean precipitation (mm/d).

for each TC, in which the maximum wind speed is at least tropical storm strength (35 kt) (e.g. Bell et al., 2000; Camargo and Sobel, 2005; Maue, 2009, 2011). The cumulative ACE of all storms in the season or a basin is a measure of the TC activity as a function of TC frequency, duration and intensity. Figure 4a shows the mean ACE per year and basin in observations and the model control simulation. Given the low ACE values in the model, we use

Table 2. Statistics of number of tropical cyclones per year for the Northern (Southern) Hemisphere from January to December (July to June) in the control run (20 yr), and observations in the period 1985–2004

	Control			Observations		
Location	Mean	%	SD	Mean	%	SD
South Indian	5.6	7.6	2.1	10.8	13.2	2.5
Australian Region	6.9	9.3	2.8	8.1	9.9	3.1
South Pacific	6.2	8.4	2.4	5.8	7.1	3.5
South Atlantic	0.2	0.3	0.4	0.1	0.1	0.2
Southern Hemisphere	18.9	25.6	5.3	24.8	28.9	4.6
North Indian	12.3	16.6	3.7	2.7	3.3	1.9
Western North Pacific	28.9	39.1	5.0	25.6	31.3	4.0
Central North Pacific	8.9	12.0	2.8	1.6	2.0	1.4
Eastern North Pacific	2.7	3.7	1.5	15.5	19.0	4.2
North Atlantic	2.2	4.2	1.5	11.9	14.2	3.6
Northern Hemisphere	55.0	74.4	8.6	57.0	69.7	6.1
Globe	73.9	100	10.2	81.8	100	8.0
North Indian*	5.8	8.6	2.1	2.7	3.3	1.9
Northern Hemisphere*	48.5	72.0	8.1	57.0	69.7	6.1
Globe*	67.4	100	9.6	81.8	100	8.0

*The North Indian Ocean TC numbers for the model were considered only for the pre-monsoon (April–June) and post-monsoon (October–December) months, excluding the monsoon season (July–September).

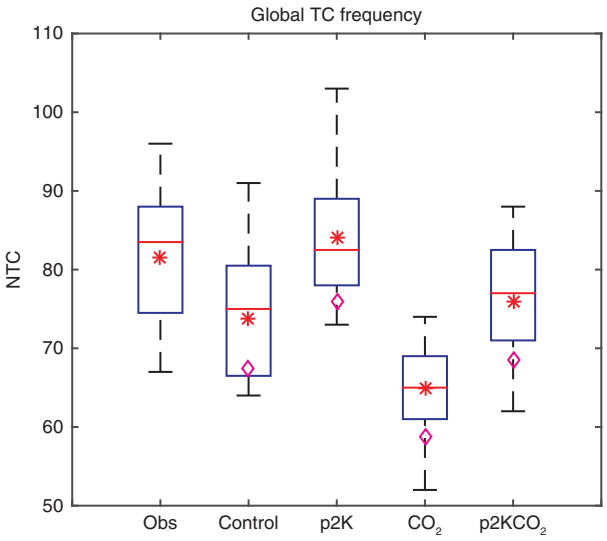

Fig. 3. Global number of tropical cyclones per year (June–July in the Southern Hemisphere basins) in observations (1984–2005), in the four GISS simulations: control, p2K, CO_2 and p2KCO_2 (as defined in Table 1). The red asterisks (*) indicate the 20-yr mean. The magenta diamonds (◇) show the 20-yr mean value when the North Indian TCs are only counted during the TC season (April–June and October–December).

here a modified version of ACE (MACE), in which all storms' wind speeds are included, without a minimum threshold, as was done previously in Camargo et al. (2005). In general, the MACE in all basins is much lower than the observed, even in the basins where the model is active. Similar to observations, the basin with the maximum MACE is the western North Pacific. The North Indian Ocean is the only basin in which the model MACE is higher than the observed ACE. This high value of MACE in the Indian Ocean is due to the occurrence of model TCs during the monsoon season, when there are none in observations. As MACE is an integrated function of frequency, lifetime and intensity, these off-season TCs (which are probably the model's version of monsoon depressions) lead to high mean value of MACE in the Indian Ocean for the whole year, as discussed above.

The low values of MACE in the model are a consequence of the low intensities reached by the model TCs, as can be seen in Fig. 5. In the top panel, we show the histograms of lifetime maximum wind speed for models and observations. The observations show a maximum between 20 and 30 m/s (tropical storm intensity) with a long tail reaching major hurricane intensity (categories 3–5). In contrast, the model distribution peaks at tropical depression intensities, with the most intense storms reaching only tropical storm intensity. For the most part, even higher resolution global climate models struggle to reach category 4–5 intensities (Murakami et al., 2012b; Murakami et al., 2015; Wehner et al., 2015); however, as shown in Shaevitz et al. (2014), the GISS model bias towards low storm intensities even when compared with models at similar resolutions. The Camargo–Zebiak detection scheme used here accounts in part for this low-intensity bias, as it detects a large number of weak storms, allowing us to study other features of the TC distribution, including the response to climate change. These results, however, should be interpreted similarly to those of lower resolution models, recognising that the model TCs are really 'TC-like vortices' much weaker, on average, than observed TCs.

The probability distribution functions of TC lifetime in the GISS model and observations (when fit to a generalised extreme value function) are given Fig. 6. The model distribution is shifted towards shorter lifetimes compared with observations. While the observations peak near 7 d, the model distribution peaks at 5 d. The model has more short-lived storms and fewer long-lived ones than are found in observations. The model bias in lifetime is relatively smaller than the biases shown in intensity. Furthermore, it is well known (Horn et al., 2014) that TC lifetime biases are very sensitive to the thresholds used in the model-tracking schemes. In the case of the western North Pacific, the model tracks tend to be longer than in observations on the northwestward direction, with a genesis shifted eastward compared with observations, while fewer model storms than observed recurve to move eastward. Overall, these two biases almost cancel each other and lead to a mean model lifetime that is not very different from observations.

The TC track density in observations and the control simulation is shown in the top panels of Fig. 7, with their difference given in panel c. The distributions of number of TCs per year in observations and the model simulations are given in Fig. 8. Analysing these figures and Table 2, some biases in the TC distribution in the GISS model can be noticed. In the Southern Hemisphere, the most active basin in the GISS model is the Australian region, while the most active in observations is the South Indian Ocean. In the Northern Hemisphere, the western North Pacific basin has a mean close to observations (28.9); however, the percentage in that basin is much higher than observations (39.1 % and 31.3 %, respectively). Similar to the central North Pacific, the North Indian Ocean is much more active in the GISS model than in observations. In contrast, the numbers of model TCs in the South Indian Ocean, the eastern North Pacific and the North Atlantic are very low. Overall, the model TC frequency is closest to that observed in the western North Pacific, the South Pacific and the Australian region.

Many global climate models have problems in simulating the correct mean number of TCs in the North Atlantic and eastern North Pacific basin. In the case of the Atlantic, this may be due to the fact that environmental conditions there

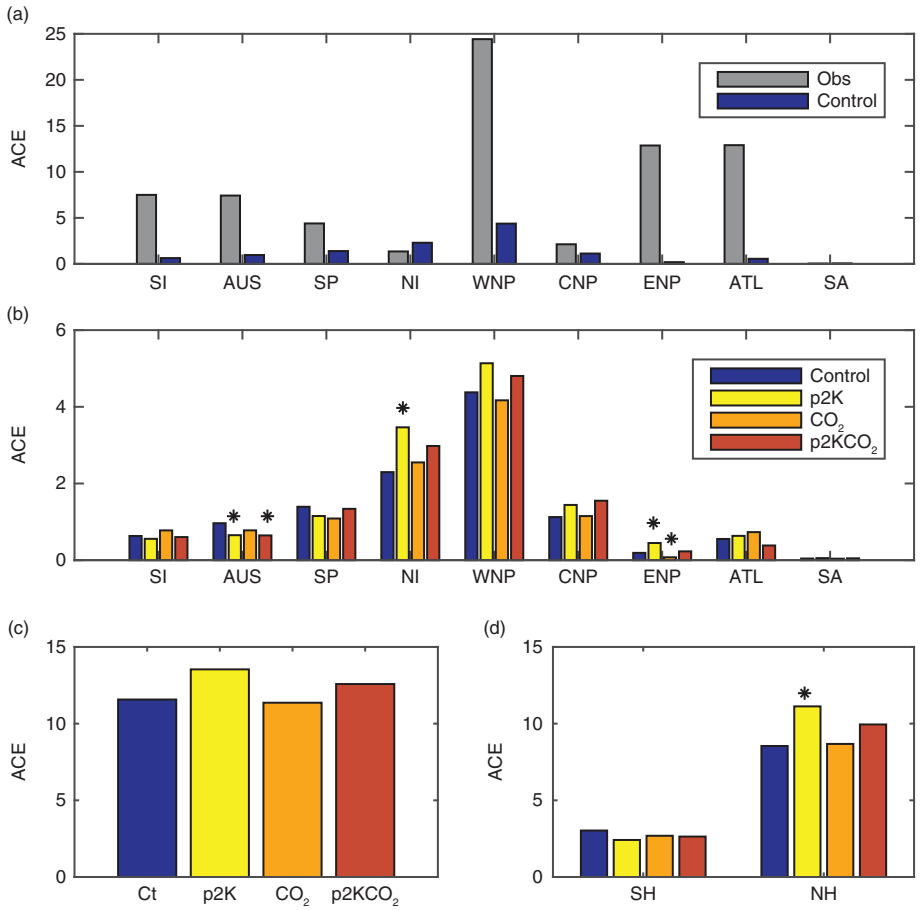

Fig. 4. (a) Mean ACE (accumulated cyclone energy, in $(m/s)^2$) in observations and MACE (modified accumulated cyclone energy) for the control run per year and per basin. Mean MACE (in $(m/s)^2$) in the four GISS simulations: control (Ct), p2K, CO_2 and $p2KCO_2$ per year: (b) per basin, (c) in the globe, and (d) per hemisphere. The abbreviations are defined as South Indian (SI), Australian (AUS), South Pacific (SP), North Indian (NI), western North Pacific (WNP), central North Pacific (CNP), eastern North Pacific (ENP), North Atlantic (ATL), South Atlantic (SA), Southern Hemisphere (SH) and Northern Hemisphere (NH). In panels b–d, statistically significant differences of MACE distributions between present and future simulations are marked with an asterisk (*), based on a Kolmogorov–Smirnov test at a 99 % significance level.

are borderline for TC formation even in reality, so even modest biases in the physics of model storm formation could easily lead to a low bias in TC frequency in that region (Camargo et al., 2005; Daloz et al., 2015). Genesis in observations in the Atlantic basin is also strongly associated with easterly waves, and models that are not able to simulate easterly waves correctly tend to have more difficulty in reproducing the TC activity in the Atlantic basin correctly (Caron and Jones, 2012; Daloz et al., 2012; Roberts et al., 2015). Another possible factor leading to biases in TC activity in models is that global climate models in general do not simulate propagating mesoscale organised convection, and that is especially important for genesis off the coast of Africa (Daloz et al., 2012). We have not evaluated these factors specifically in the GISS model.

The poor simulation of TC activity in the eastern North Pacific is common to many low-resolution models and has been associated with a variety of factors: the small size of the basin, with a very high TC genesis density in that small area during the season; the proximity to the Central American mountains, which coarse model grids do not resolve, and the difficulty of the models in simulating easterly waves crossing from the Atlantic into the eastern Pacific (Bengtsson et al., 2007).

The seasonality of TC frequency in observations and in the model simulations is given in Fig. 9. The month at which the maximum value of TCs occurs in the model is later than that in observations, in the Australian region (February in observations and March in the model) and western North Pacific (August in observations and October in the model). Overall, the model is active at the right times of year in most basins, with the prominent exception of the North Indian Ocean. In that basin, in observations,

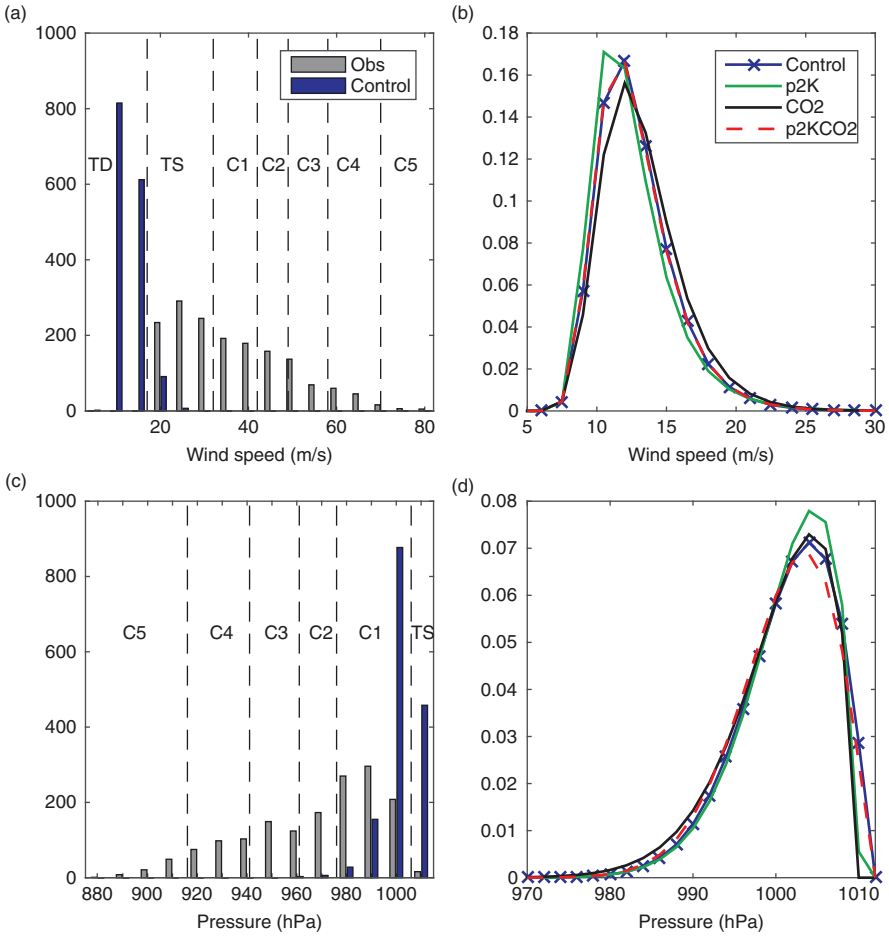

Fig. 5. Histogram of the lifetime maximum intensity for maximum wind speed (in m/s, (a)) and minimum surface pressure (in hPa, (c)) in observations (grey bars) and the control simulation (blue bars). The vertical lines show the thresholds separating the tropical depression (TD), tropical storm (TS) and Saffir–Simpson categories 1–5 (C1–C5). TC lifetime maximum intensity [wind speed in m/s (b) and surface pressure in hPa (d)] probability distribution functions, obtained by fitting the data to a generalised extreme value distribution, for the four GISS simulations: control, p2K, CO_2 and p2KCO_2.

there are two seasons, pre-monsoons and post-monsoons, with a minimum during the monsoon season. The model has one single peak with a maximum in September. As already discussed, this is a common bias in many models (e.g. Camargo et al., 2005; Shaevitz et al., 2014) and is probably due to the inability of the model and/or the tracking scheme to distinguish between TCs and monsoon depressions.

4. TC activity in future climates

In this section, we will examine how the model TC activity changes in the various climate change experiments. The global mean number of storms in the model increases 14.5 % in the p2K simulation, decreases 10.5 % in the CO_2 simulation and decreases slightly (4 %) in the p2KCO_2 experiment (see Fig. 3). The differences between the global NTC distributions of the control simulation and the p2K and CO_2 simulations are statistically significant using a t-test and a rank sum test at the 99 % significance level and the Kolmogorov–Smirnov test at the 95 % level. The difference in the global NTC distribution between the control and the p2KCO_2 simulations is not statistically significant. The value in the p2KCO_2 experiment is almost exactly the sum of those from the p2K and CO_2 experiments. This linearity is found in other models as well, though the signs of the changes for a specific forcing scenario are not consistent across all models. The results from the HiRAM model, for example, show a 10 % decrease in both the p2K and CO_2 simulations, with a total decrease of 20 % in the p2KCO_2 experiment (Held and Zhao, 2011), similar to previous results by Yoshimura and Sugi (2005), and most models from the HWG (Zhao et al., 2013; Walsh et al., 2015), though not all (Horn et al., 2014).

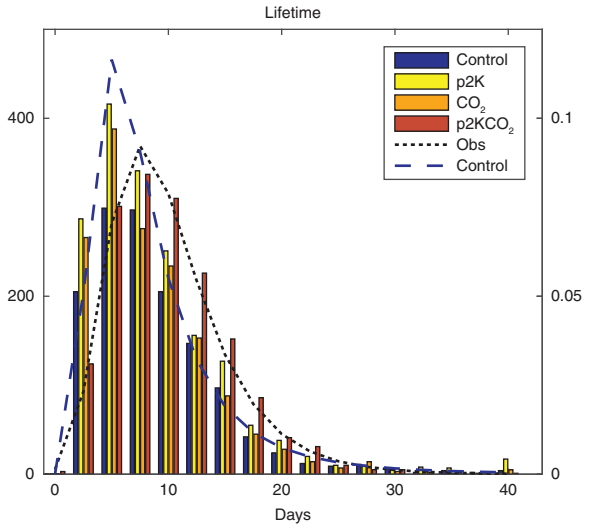

Fig. 6. Histogram of TC lifetime (days) for the four GISS simulations: control, p2K, CO_2 and p2KCO_2 (bars and left vertical axis). TC lifetime probability distribution functions, obtained by fitting the data to a generalised extreme value distribution, for observations (black dotted line, right vertical axis) and the control simulation (blue dashed line, right vertical axis).

The global frequency increase in the p2K simulation is due to large increases in TC frequency in the North Indian Ocean and all three basins of the North Pacific (see Figs. 8c and 7). In the Southern Hemisphere, there is actually a decrease in TC activity in the p2K simulation in all three basins, in particularly in the South Indian Ocean and near Australia as shown in Figs. 8 and 7d. Similarly, the global decrease in NTC in the CO_2 simulation is mainly due to decreases in NTC in the whole Pacific (North and South), with very small NTC changes in the other basins (Fig. 8), due to an incoherent pattern in those basins (Fig. 7d and e). The very small change in global NTC in the p2KCO_2 experiment is present in all basins, with exception of Australia, where there is a decrease in NTC (Fig. 8). However, specific subregions seem to exhibit large differences in that case, in particular, an increase in TC activity in the central North Pacific and in the western North Pacific near the Asian continent, with a decrease in TC occurrence between these two maxima (Fig. 7f). In the Southern Hemisphere, decrease in TC activity is restricted to the eastern coast of Australia.

The seasonality of the TC frequency in the climate change simulations is shown in Fig. 9. The most notable difference in the NTC per month between the control and climate change runs is the occurrence of higher levels of mean TC activity in most months in the p2K and p2KCO_2 simulations in the Pacific basins and the North Indian Ocean in both hemispheres. There is no significant change in the NTC seasonality in the future runs in any of the basins. The central North Pacific seasonal cycle is slightly delayed in the p2K and CO_2 scenarios, but these changes are not statistically significant.

Consistent with the higher frequency of TCs in the Northern Pacific basins and North Indian Ocean in the p2K and p2KCO_2 simulation, there are higher values of MACE on those basins (Fig. 4b). In the Southern Hemisphere basins, MACE slightly decreases in all cases in the South Pacific and Australian basins, while in the South Indian Ocean MACE slightly increases in the CO_2 simulation and remains almost constant in the two other cases. Only in very few cases the MACE changes in the future scenarios are statistically significant (at the 99 % significance level using the Kolmogorov–Smirnov test); these cases are marked with asterisks in Fig. 4b. The MACE changes overall, globally and considering all experiments, are very small. The very low MACE values could be potentially contributing to these very small changes.

The probability distribution functions of lifetime maximum intensity are given in Fig. 5b. There is a statistically significant (using the Kolmogorov–Smirnov test at 99 % significance level) shift towards weaker (stronger) TCs in the p2K (CO_2) scenario. These shifts are only significantly different from the control for the whole distribution, with no significant changes in the values of the most intense storms (tail of the distributions).

The lifetime distribution (Fig. 6) in the p2K future simulation is statistically significant different than the control case (95 % level, Kolmogorov–Smirnov test), with almost no change for the other two future scenarios. There is a slight shift towards longer-lived storms in the CO_2 case.

5. Environmental fields

In this section, a few large-scale environmental fields usually associated with TC activity are shown. In each case, the model climatology for the control simulation (panel b in all figures) is compared with the same climatological field in reanalysis or observations (panel a), by showing both climatologies and their difference (panel c). The differences in the fields in the climate change simulations compared with control are also shown (panels d, e and f). In all figures and panels in this section, August–October (ASO) climatological means are shown in the Northern Hemisphere and January–March (JFM) in the Southern Hemisphere, as these are the peak TC seasons in each hemisphere.

The PI is a theoretical limit for TC intensity (Emanuel, 1988) and is calculated as a function of SST, sea level pressure and profiles of temperature and humidity. Changes in PI can be used as a proxy for changes in TC intensity, especially in low-resolution climate models (Vecchi and Soden, 2007; Camargo, 2013), as variations in the local PI are significantly correlated with those in actual TC intensities on a range of time and space scales (Emanuel, 2000;

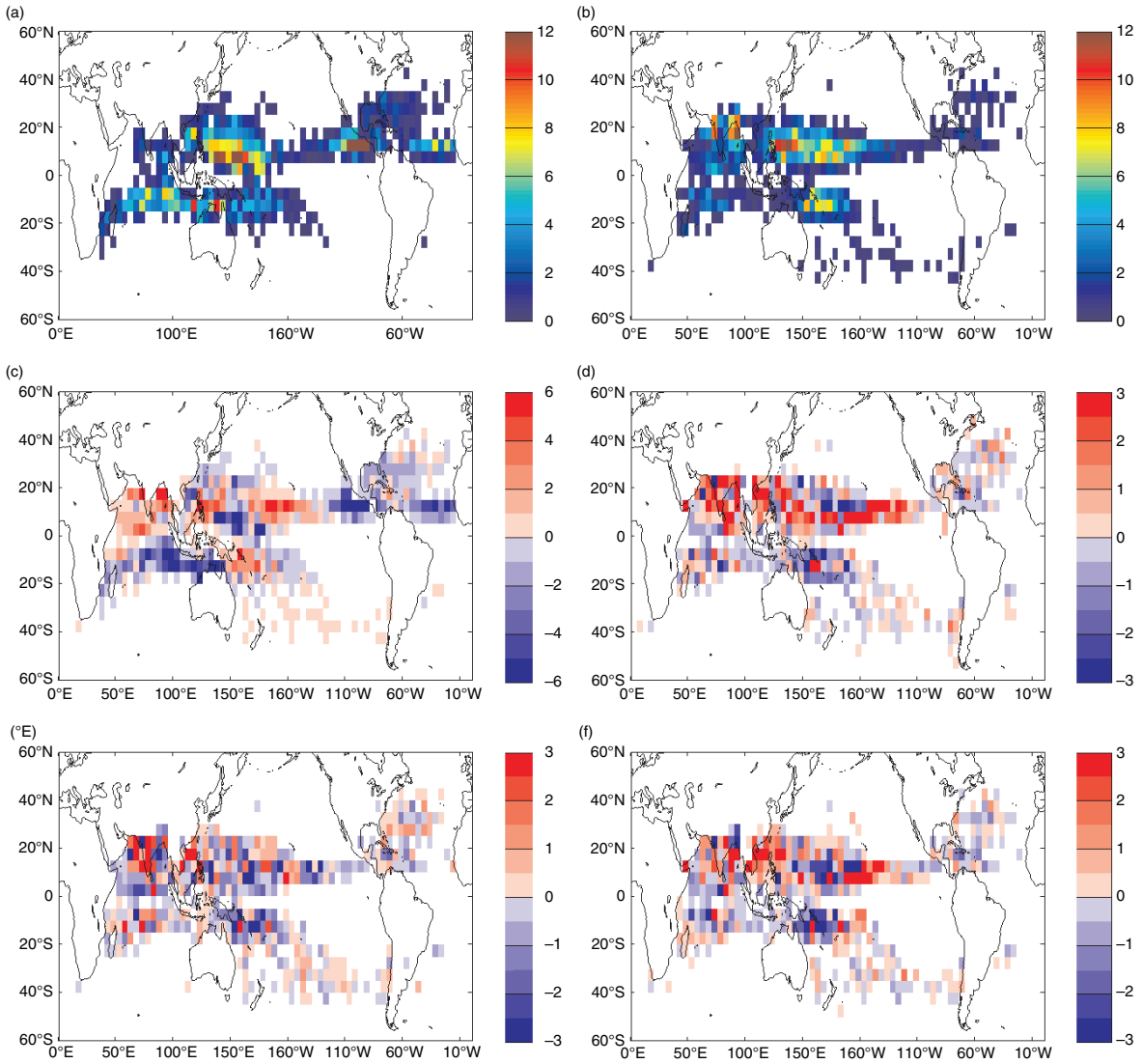

Fig. 7. Track density (mean count of TC passages per grid point) in (a) observations and (b) the control simulation. Track density differences between (c) control and observations, (d) p2K and control, (e) CO_2 and control, and (f) p2KCO_2 and control.

Wing et al., 2007; Kossin and Camargo, 2009). The PI is regularly used as one of the variables in genesis indices (Camargo et al., 2007a; Emanuel, 2010; Camargo et al., 2014) as well as the ventilation index (Tang and Emanuel, 2012; Tang and Camargo, 2014), and therefore has some connection to TC frequency as well.

The PI climatology pattern produced by the GISS ModelE2 in the control experiment is quite similar to that in the ERA-Interim reanalysis (see Fig. 10a and b). However, the simulated values of PI tend to be higher than those in reanalysis over the western Pacific and Indian Oceans (Fig. 10c), while in the main development region of the North Atlantic and most of the eastern Pacific, the simulated PI is lower than that in reanalysis. The PI increases almost uniformly in the tropics in both the p2K and p2KCO_2 simulations (Fig. 10d and f). These increases in PI are not associated with increases in the model TC intensities, however (Fig. 5). We suspect that the model TC intensities are fundamentally limited by resolution and model physics to the extent that they cannot increase in response to modest PI increases.

Figure 11 shows the magnitude of the vertical wind shear in ERA-Interim reanalysis and the simulations. The pattern of the vertical shear is quite similar to that of the reanalysis. The magnitude of the shear is lower in the model in most of the northern Pacific and Indian Ocean and in the South Indian and South Pacific North of 20°S, however. These are the same regions where the model is most active. In contrast, the magnitude of the shear is too high along two diagonal bands: one that starts in Hawaii and continues

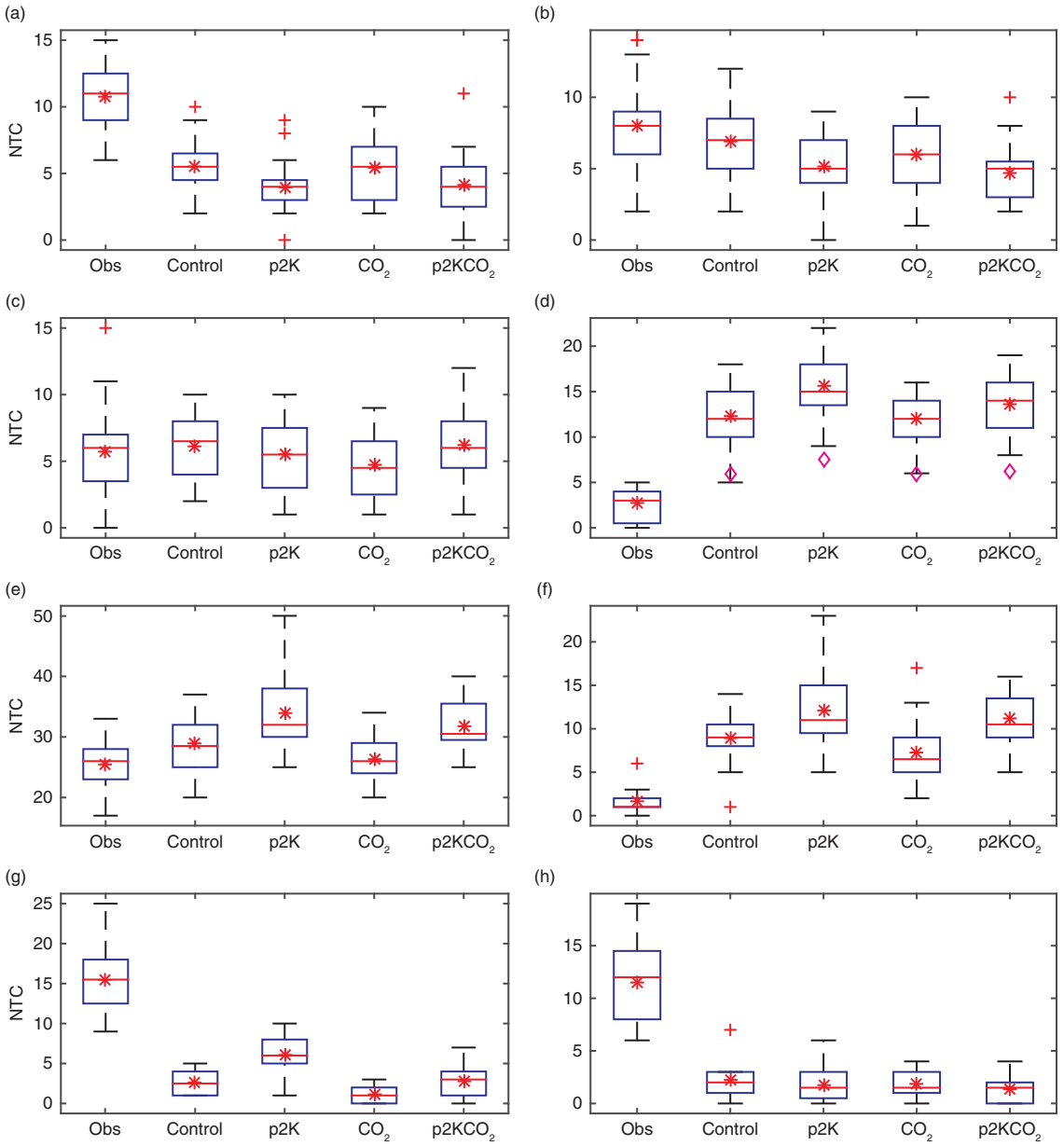

Fig. 8. Number of tropical cyclones per year in observations and in the four GISS simulations: control, p2K, CO_2 and $p2KCO_2$ per basin in (a) South Indian Ocean, (b) Australian Region, (c) South Pacific, (d) North Indian Ocean, (e) western North Pacific, (f) central North Pacific, (g) eastern North Pacific and (h) North Atlantic. The red asterisks indicate the 20-yr mean. The magenta diamonds (◇) in panel d show the 20-yr mean value when the North Indian TCs are only counted during the TC season (April–June and October–December).

through part of the Gulf of Mexico and United States east coast, while the second stretches from the South Indian Ocean across the South Pacific into the South Atlantic. These regions with high shear biases tend to have biases towards low TC frequency: the eastern Pacific, North Atlantic and South Indian Ocean. In the Atlantic, there is also a region of anomalous high shear near Africa, over the main development region, which might help explain the very low bias in TC frequency in that basin.

In the climate change simulations (Fig. 11d–f), there is a small decrease in the magnitude of the vertical shear in most of the northern Pacific, North Indian Ocean and South Pacific (North of 20S) in the p2K and $p2KCO_2$ simulations. The biggest decreases occur in the North Indian Ocean, where there is an increase in TC activity in those two simulations. In the North Atlantic and eastern North Pacific, there is a mix of regions in which the vertical shear increases and decreases. In the p2K and $p2KCO_2$

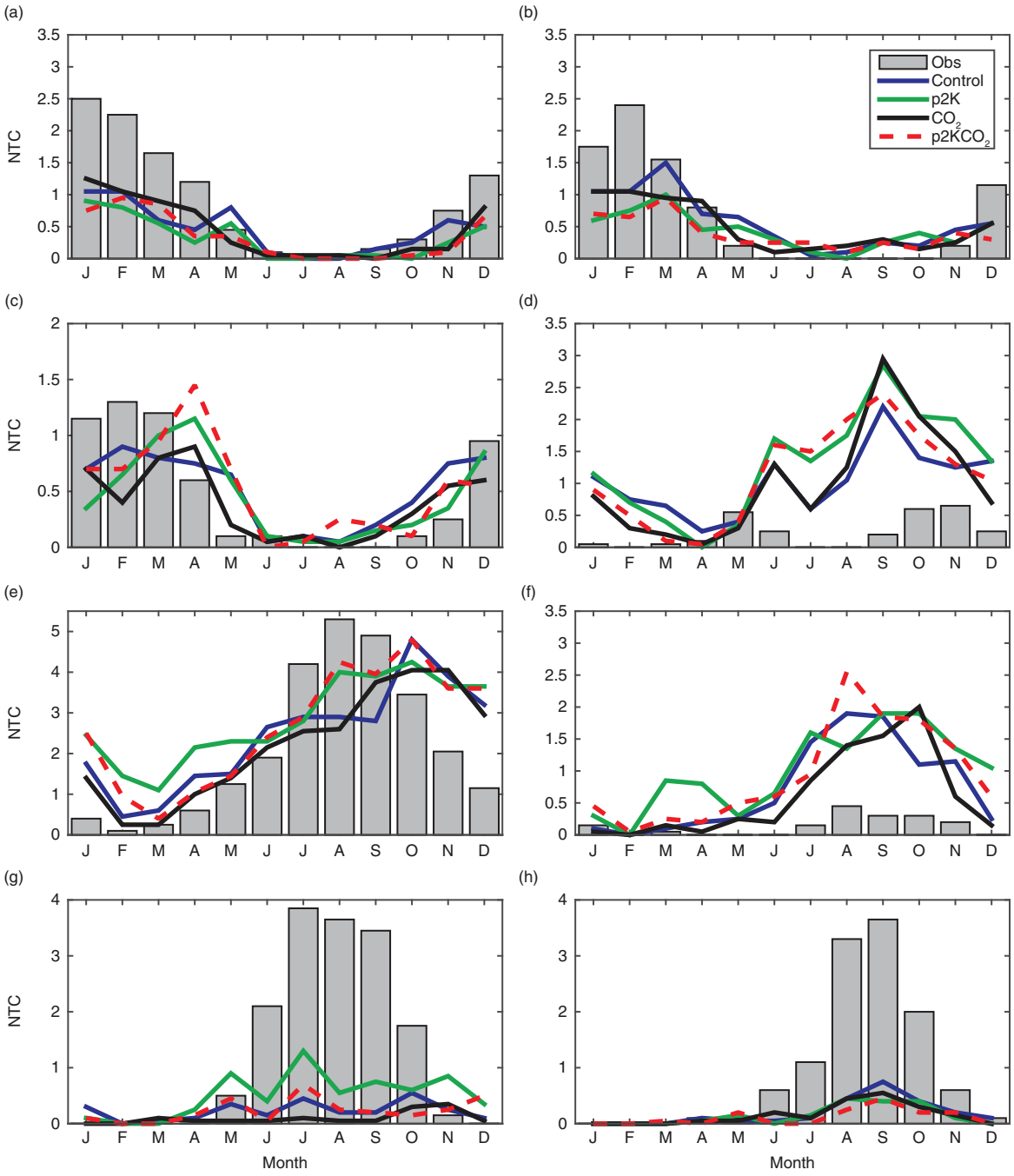

Fig. 9. Mean number of tropical cyclones per month and per basin in observations (1984–2005), in the four GISS simulations: control, p2K, CO_2 and p2KCO_2 in (a) South Indian Ocean, (b) Australian Region, (c) South Pacific, (d) North Indian Ocean, (e) western North Pacific, (f) central North Pacific, (g) eastern North Pacific and (h) North Atlantic.

simulations, the increase in vertical shear in the North Atlantic and eastern Pacific occurs in regions in which the model climatologically has a bias towards high shear, making those regions even more unfavourable for TC formation.

Figure 12 examines the relative humidity at mid-levels (600 hPa) in the GISS model. While the 600 hPa relative humidity of the model is too low compared with reanalysis (Fig. 12c), the column relative humidity is too high (not shown). This difference can be explained by comparing the vertical profile of the mean tropical relative humidity in the GISS model and the ERA-Interim reanalysis (not shown). While the relative humidity is slightly larger in the GISS

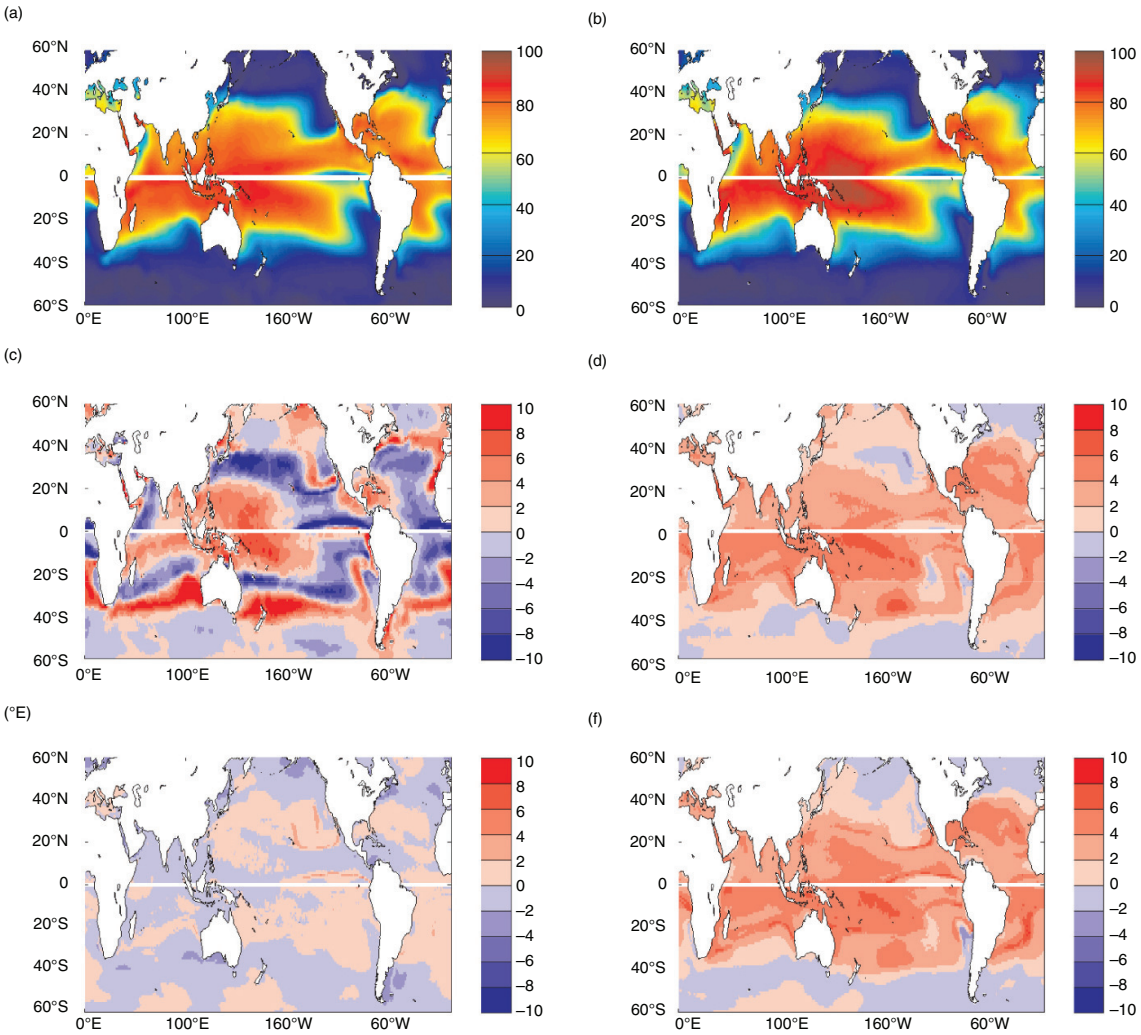

Fig. 10. Potential intensity (m/s) in (a) the ERA-Interim reanalysis and (b) the control simulation. Potential intensity differences between (c) control and ERA-Interim reanalysis, (d) p2K and control, (e) CO_2 and control, and (f) p2KCO_2 and control. In all panels, August–October (ASO) seasonal means are shown in the Northern Hemisphere and January–March (JFM) means in the Southern Hemisphere.

model than in the reanalysis below 700 hPa, the GISS model is drier in mid-levels. Given that the lower levels have a higher contribution to integrated column relative humidity, this explains the different signs of the biases of the 600 hPa and column relative humidity.

However, the changes in the 600 hPa (Fig. 12d–f) and column relative humidity (not shown) with climate change are very similar, with increases in the western North Pacific near Asia and in the eastern North Pacific from California to Hawaii, as well as in the South Indian Ocean, in both p2K and p2KCO_2 simulations. In the CO_2 case, increases in the northern Pacific and South Indian Ocean occur over smaller regions, with parts of those basins experiencing decreases. In the Bay of Bengal (in particular, further from the Indian continent), the humidity decreases in all three simulations, but there is a large increase in the Arabian Sea North of 10°N. In the North Atlantic, there is an increase in the 10°N to 20°N band in both p2K and p2KCO_2 simulations, while in the CO_2 simulation the reduction occurs in the whole Atlantic basin. The fact that the CO_2 simulation is drier where the model is usually most active – in particular, over a large part of the western North Pacific – probably helps explain why the model produces fewer TCs globally in that simulation.

We also examined the TCGI in the ERA-Interim reanalysis and the GISS model (Fig. 13), based on the Tippett et al. (2011) technique and using the formulation of the index that depends on the PI and saturation deficit as discussed in Camargo et al. (2014). The regression coefficients were obtained for the ERA-Interim reanalysis fields and observations and used without modification for the GISS model. Though the pattern of the GISS model TCGI

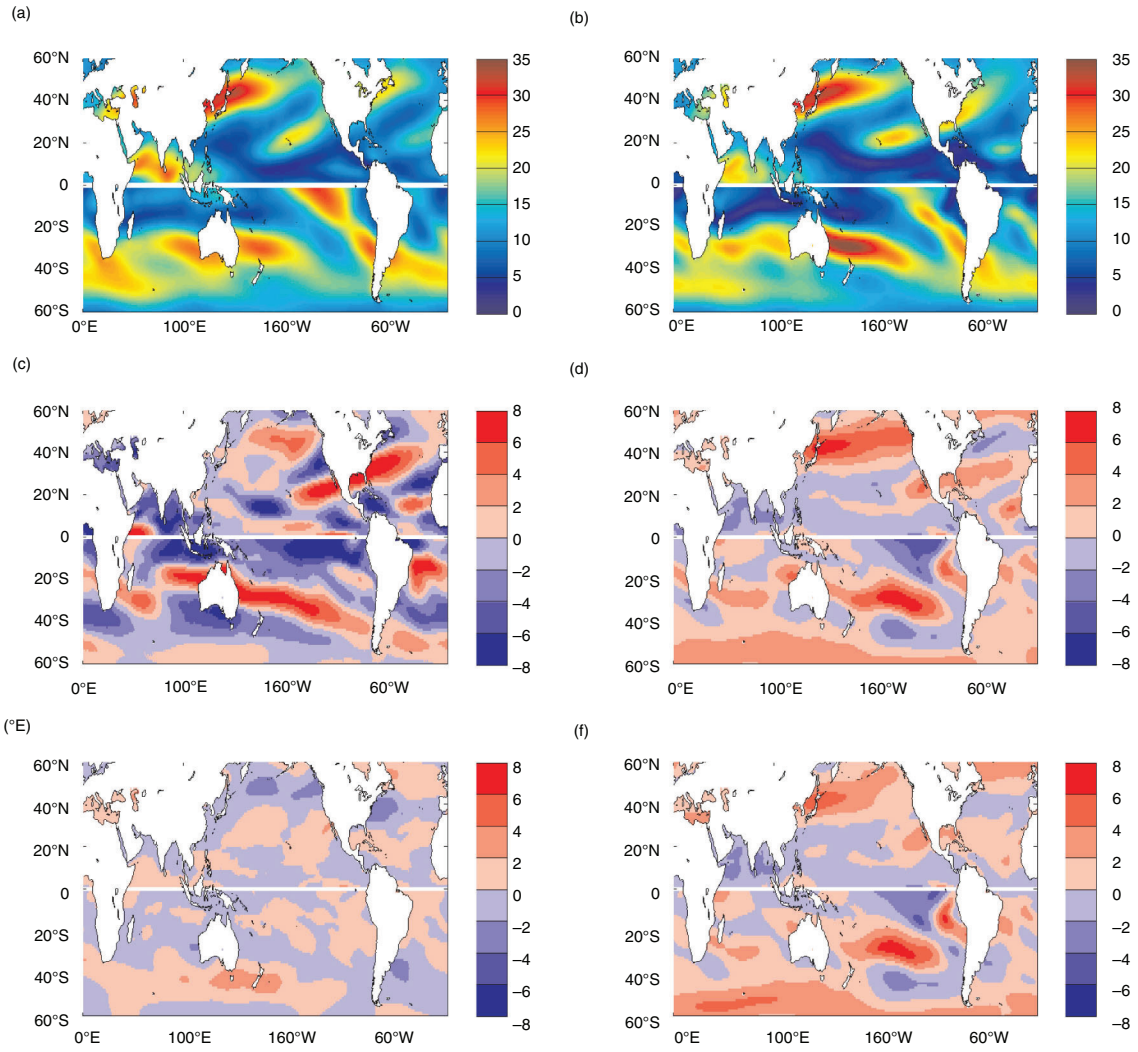

Fig. 11. Magnitude of the climatological mean vertical wind shear (200 hPa minus 850 hPa, in m/s) in (a) the ERA-Interim reanalysis and (b) the control simulation. Vertical winds shear magnitude differences between (c) control and ERA-Interim reanalysis, (d) p2K and control, (e) CO_2 and control, and (f) p2KCO_2 and control. In all panels, ASO (JFM) is shown in the Northern (Southern) Hemisphere.

in the simulated present climate is quite similar to that in ERA-Interim reanalysis, the magnitude of the model TCGI is much larger than that in the reanalysis. The reason for this discrepancy can be explained by the bias in the saturation deficit, similar to that mentioned for the column relative humidity. The saturation deficit bias has a significant effect on the total magnitude of the TCGI, in particular in the western North Pacific where the model TCs are most active. Therefore, we show here in Fig. 13 the TCGI for the GISS model normalised so that the mean total number of storms (sum of TCGI for all months and all grid points) climatologically are the same.

By comparing Fig. 13a with Fig. 7a and 1a, we note a few biases in the TCGI in the ERA-Interim reanalysis, in particular low values of the TCGI in the eastern North Pacific and higher values in the South Pacific than in the South Indian Ocean, which is the opposite from what occurs in the observations. In the case of the GISS model (comparing Fig. 13b with Figs. 7b and 1b), the TCGI captures the maximum activity in the western Pacific Ocean in both hemispheres, as well as the low level of activity in the eastern North Pacific and North Atlantic. However, the anomalously high model TC frequency in the central North Pacific and North Indian Ocean model is not represented by the model TCGI.

The differences in TCGI in the future runs (Fig. 13d–f) may partly explain the changes in TC frequency in the model. The largest increase in TCGI in the p2K and p2KCO_2 simulation occur in the western North Pacific, where the largest increases in the TC frequency occur.

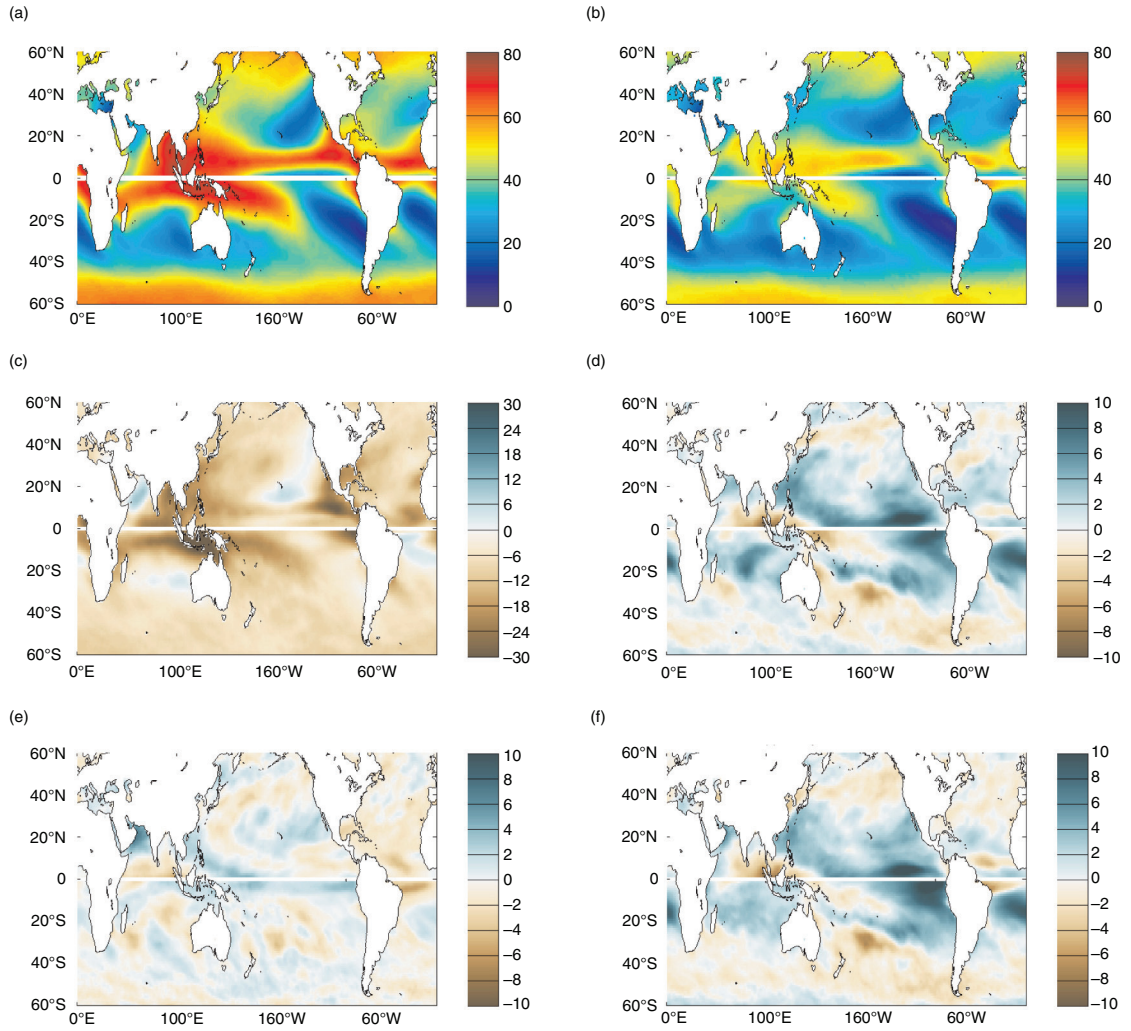

Fig. 12. Climatological mean relative humidity (in%) at 600 hPa in (a) the ERA-Interim reanalysis and (b) the control simulation. Relative humidity 600 hPa differences between (c) control and ERA-Interim reanalysis, (d) p2K and control, (e) CO_2 and control, and (f) p2KCO_2 and control. In all panels, ASO (JFM) is shown in the Northern (Southern) Hemisphere.

In contrast, in the CO_2 simulation there is a reduction of TCGI in that region of the Pacific. The TCGI is reduced in most of the Atlantic in all three climate change simulations, especially in the p2KCO2 simulation. The changes in TCGI in the Southern Hemisphere are much smaller than in the northern Indo-Pacific region, in the p2K and p2KCO_2 simulations, similarly to what occurs with the TC frequency in the model. There are some discrepancies, for instance, although there is an increase in the number of TCs in the model in the North Indian Ocean for the p2KCO_2 scenario, the TCGI decreases in that region, similarly to the western part (100°E–120°E) of the western North Pacific. The discrepancy in the North Indian Ocean could potentially be related to the inability to distinguish between monsoon depressions and TCs in that region.

6. Conclusions

At $1^\circ \times 1^\circ$ horizontal resolution, the GISS ModelE2 still performs similarly to lower resolution climate models, in that it produces relatively weak TC-like vortices. We analyse it using a detection and tracking scheme which accounts for that, setting thresholds for detection which are lower than those observed. With this accommodation, the GISS model is able to replicate various characteristics of the observed TC characteristics, such as the global number of TCs, a higher number of TCs in the Northern Hemisphere and a lifetime distribution with a peak around 10 d. The regional characteristics of TC activity still have significant biases, however. In particular, the model is too active in the central North Pacific and North Indian Ocean and does not produce enough TCs in the eastern

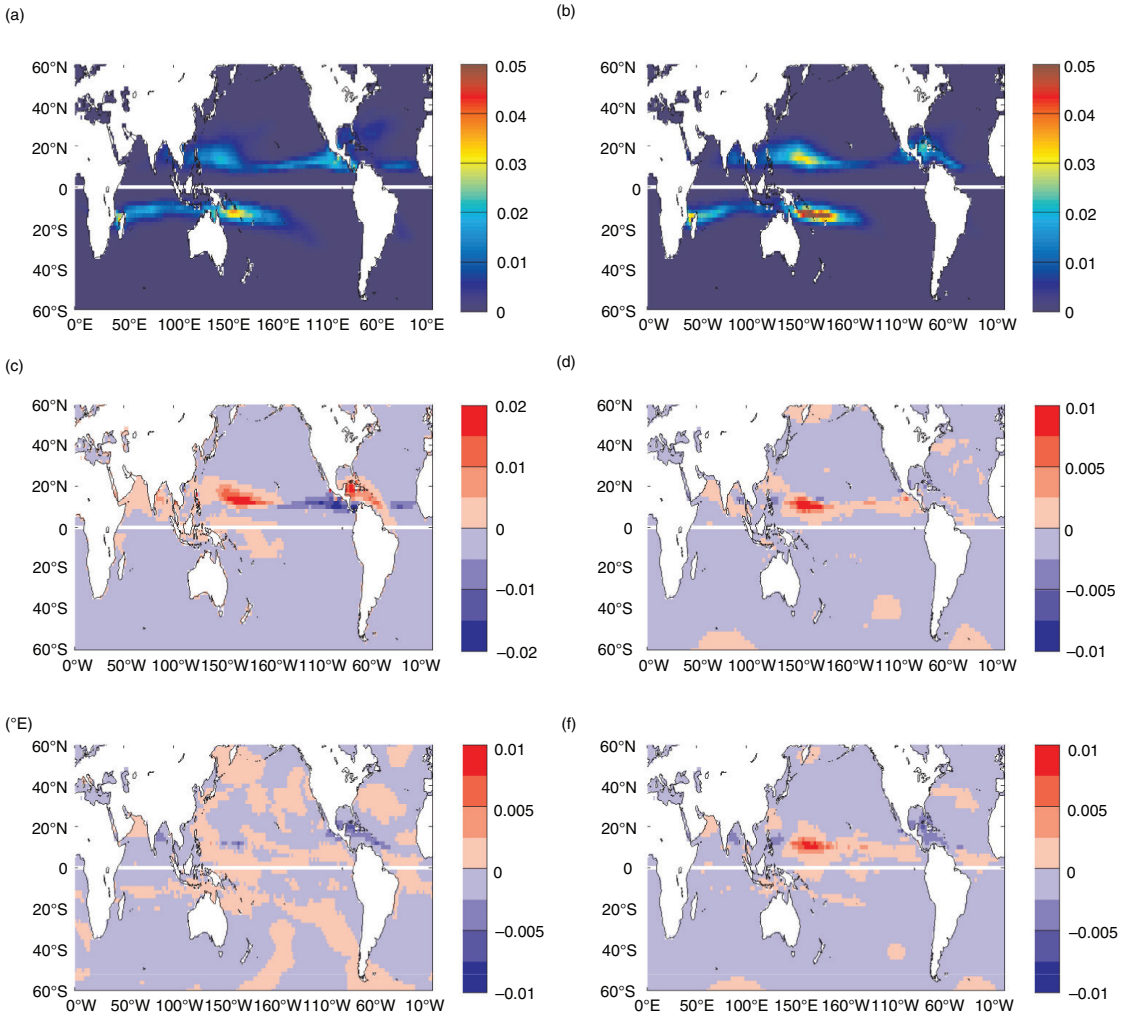

Fig. 13. Climatological mean Tropical Cyclone Genesis Index (TCGI; mean number of TC genesis per year per grid point) in (a) the ERA-Interim reanalysis and (b) the control simulation. TCGI differences between (c) control and ERA-Interim reanalysis, (d) p2K and control, (e) CO_2 and control, and (f) p2KCO_2 and control. In all panels, ASO (JFM) is shown in the Northern (Southern) Hemisphere. The model TCGI in all simulations has been normalised by the ratio of the integrated value of the annual TCGI in the control and ERA-Interim.

North Pacific, North Atlantic and South Indian Ocean. Many of these biases are common in models with similar and lower horizontal resolution. The characteristic of the model that has the largest bias, even compared with models of similar horizontal resolution, is the model intensity, which is too low overall.

Global TC frequency increases in the p2K simulation and decreases in the CO_2 simulation, while these two signals approximately cancel, resulting in almost no change in the global TC frequency, in the p2KCO_2 simulation. These changes in the global TC frequency are mostly due to changes in the Northern Pacific and North Indian basins, with much smaller changes in the other regions. These results are similar to Yoshimura and Sugi (2005) and Held and Zhao (2011), in that the p2KCO_2 TC global frequency change corresponds approximately to a linear sum of those from the p2K and CO_2 simulations, but differs in that the effects of CO_2 and SST increases oppose each other here, whereas both lead to frequency reductions in Yoshimura and Sugi (2005) and Held and Zhao (2011). While there is no significant change in TC intensity in the future runs, there are increases in MACE in these basins, reflecting the changes in TC frequency. These results are in contrast with other global climate models' simulations, which tend to have a slight decrease in TC frequency and an increase in the occurrence of the most intense storms in global warming simulations (Knutson et al., 2010; Walsh et al., 2015).

The GISS model climatologies of PI and vertical shear have patterns very similar to those derived from the ERA-Interim reanalysis. The biases in these two quantities, however, may partly explain the biases in TC activity in the model, in particular in the North Atlantic, where the model PI is too low and the vertical shear too high in most of the basin. In contrast, in the western North Pacific, where the model TCs are most active, the PI has a high bias and the vertical shear a low bias.

Projections of TC activity with the GISS model in 1° horizontal resolution in future climates have to be considered carefully. Recent papers have shown that TC projections are strongly dependent on horizontal resolution (e.g. Strachan et al., 2013; Wehner et al., 2015). The progress that has been made in this field in the last few years is enormous, as discussed in Camargo and Wing (2016). The GISS model now has resolution high enough so that its TC activity could be analysed in detail. We hope that in the next generations of the model, studies like this will help improve the quality of the TC climatology in the GISS model leading to more reliable TC projections.

7. Acknowledgements

The authors acknowledge the support from the following grants: NASA NNX09AK34G, NNX13AM18G, NSF AGS 1143959 and a NASA Modelling and Analysis Program RTOP at NASA/GISS. The authors thank the members of the US CLIVAR Hurricane Working Group (HWG). They also thank Naomi Henderson for making the model data available for the HWG and managing the HWG data set. The model data used here can potentially be made available by individual requests.

References

Allen, J. T., Tippett, M. K. and Sobel, A. H. 2015a. An empirical model relating US monthly hail occurrence to large-scale meteorological environment. *J. Adv. Model. Earth Syst.* **7**, 226–243.

Allen, J. T., Tippett, M. K. and Sobel, A. H. 2015b. The influence of El Niño/Southern Oscillation on tornado and hail frequency in the United States. *Nat. Geosci.* **8**, 278–283.

Bell, G. D., Halpert, M. S., Schnell, R. C., Higgins, R. W., Lawrimore, J. and co-authors. 2000. Climate assessment for 1999. *Bull. Am. Meteorol. Soc.* **81**, S1–S50.

Bengtsson, L., Botzet, M. and Esch, M. 1995. Hurricane-type vortices in a general circulation model. *Tellus A.* **47**, 175–196.

Bengtsson, L., Hodges, K. I. and Esch, M. 2007. Tropical cyclones in a T159 resolution global climate model: comparison with observations and re-analysis. *Tellus A.* **59**, 396–416.

Bister, M. and Emanuel, K. A. 1998. Dissipative heating and hurricane intensity. *Meteorol. Atmos. Phys.* **52**, 233–240.

Bister, M. and Emanuel, K. A. 2002a. Low frequency variability of tropical cyclone potential intensity. 1. Interannual to interdecadal variability. *J. Geophys. Res.* **107**, 4801.

Bister, M. and Emanuel, K. A. 2002b. Low frequency variability of tropical cyclone potential intensity. 2. Climatology for 1982–1995. *J. Geophys. Res.* **107**, 4621.

Bretherton, C. S., Peters, M. E. and Back, L. E. 2004. Relationships between water vapour path and precipitation over the tropical oceans. *J. Clim.* **17**, 1517–1528.

Camargo, S. J. 2013. Global and regional aspects of tropical cyclone activity in the CMIP5 models. *J. Clim.* **26**, 9880–9902.

Camargo, S. J. and Barnston, A. G. 2009. Experimental seasonal dynamical forecasts of tropical cyclone activity at IRI. *Weather Forecast.* **24**, 472–491.

Camargo, S. J., Barnston, A. G. and Zebiak, S. E. 2005. A statistical assessment of tropical cyclones in atmospheric general circulation models. *Tellus A.* **57**, 589–604.

Camargo, S. J., Emanuel, K. A. and Sobel, A. H. 2007a. Use of a genesis potential index to diagnose ENSO effects on tropical cyclone genesis. *J. Clim.* **20**, 4819–4834.

Camargo, S. J. and Sobel, A. H. 2005. Western North Pacific tropical cyclone intensity and ENSO. *J. Clim.* **18**, 2996–3006.

Camargo, S. J., Sobel, A. H., Barnston, A. G. and Emanuel, K. A. 2007b. Tropical cyclone genesis potential index in climate models. *Tellus A.* **59**, 428–443.

Camargo, S. J., Tippett, M. K., Sobel, A. H., Vecchi, G. A. and Zhao, M. 2014. Testing the performance of tropical cyclone genesis indices in future climates using the HIRAM model. *J. Clim.* **27**, 9171–9196.

Camargo, S. J. and Wing, A. A. 2016. Tropical cyclones in climate models. *WIREs Clim. Change.* **7**, 211–237, DOI: http://dx.doi.org/10.1002/wcc373

Camargo, S. J. and Zebiak, S. E. 2002. Improving the detection and tracking of tropical storms in atmospheric general circulation models. *Weather Forecast.* **17**, 1152–1162.

Caron, L.-P. and Jones, C. G. 2012. Understanding and simulating the link between African Easterly Waves and Atlantic tropical cyclones using a regional climate model: the role of domain size and lateral boundary condition. *Clim. Dynam.* **39**, 113–135.

Chu, J.-H., Sampson, C. R., Levine, A. S. and Fukada, E. 2002. *The Joint Typhoon Warning Center Tropical Cyclone Best-Tracks, 1945–2000*. Technical Report. NRL/MR/7540-02-16, Naval Research Laboratory. Online at: http://www.usno.navy.mil/NOOC/nmfc-ph/RSS/jtwc/best_tracks/TC_bt_report.html

Collins, W. D., Ramaswamy, V., Schwarzkopf, M. D., Sun, Y., Portmann, R. W. and co-authors. 2006. Radiative forcing by well-mixed greenhouse gases: estimates from climate models in the Intergovernmental Panel on Climate Change (IPCC) Fourth Assessment Report (AR4). *J. Geophys. Res.* **111**, D14317.

Corbosiero, K. L., Molinari, J. and Aiyyer, A. R. 2006. The structure and evolution of Hurricane Elena (1985). Part II: convective asymmetries and evidence for vortex Rossby waves. *Mon. Weather Rev.* **134**, 3073–3090.

Daloz, A. S., Camargo, S. J., Kossin, J. P., Emanuel, K., Horn, M. and co-authors. 2015. Cluster analysis of explicitly and downscaled simulated North Atlantic tropical cyclone tracks. *J. Clim.* **28**, 1333–1361.

Daloz, A. S., Chauvin, F., Walsh, K., Lavender, S., Abbs, D. and co-authors. 2012. The ability of general circulation models to simulate tropical cyclones and their precursors over the Atlantic main development region. *Clim. Dynam.* **39**, 1559–1576.

Dee, D. P., Uppala, S. M., Simmons, A. J., Berrisford, P., Poli, P. and co-authors. 2011. The ERA-Interim reanalysis: configuration and performance of the data assimilation system. *Q. J. Roy. Meteorol. Soc.* **137**, 553–597.

Del Genio, A. D. and Yao, M.-S. 1993. Efficient cumulus parameterization for long-term climate studies: the GISS scheme. In: *The Representation of Cumulus Convection in Numerical Models* (eds. K. A. Emanuel, and D. A. Raymond) Vol. 46 of Meteorological Monographs, American Meteorological Society, Boston, MA, pp. 181–184.

Del Genio, A. D., Yao, M.-S., Kovari, W. and Lo, K. K. 1996. A prognostic cloud water parameterization for general circulation models. *J. Clim.* **9**, 270–304.

Ditchek, S. D., Boos, W. R., Camargo, S. J. and Tippett, M. K. 2016. A genesis index for monsoon disturbances. *J. Clim.* **29**, 5189–5203. DOI: http://dx.doi.org/10.1175/JCLI-D-15-0704.1

Elsner, J. B., Strazzo, S. E., Jagger, T. H. and LaRow, T. 2013. Sensitivity of limiting hurricane intensity to SST in the Atlantic from observations and GCMs. *J. Clim.* **26**, 5946–5957.

Emanuel, K. 2010. Tropical cyclone activity downscaled from NOAA-CIRES reanalysis, 1908–1958. *J. Adv. Model. Earth Syst.* **2**, 1. DOI: http://dx.doi.org/10.3894/JAMES.2010.2.1

Emanuel, K. A. 1988. The maximum intensity of hurricanes. *J. Atmos. Sci.* **45**, 1143–1155.

Emanuel, K. A. 1995. Sensitivity of tropical cyclones to surface exchange coefficients and a revised steady-state model incorporating eye dynamics. *J. Atmos. Sci.* **52**, 3969–3976.

Emanuel, K. A. 2000. A statistical analysis of tropical cyclone intensity. *Mon. Weather Rev.* **128**, 1139–1152.

Hansen, J., Ruedy, R., Lacis, A., Sato, M., Nazarenko, L. and co-authors. 2000. Climate modelling in the global warming debate. In: *General Circulation Model Development* (ed. D. Randall) Academic Press, San Diego, CA, pp. 127–174.

Hansen, J., Sato, M., Ruedy, R., Nazarenko, L., Lacis, A. and co-authors. 2005. Efficacy of climate forcings. *J. Geophys. Res.* **110**, D18104.

Hansen, J. E., Russell, G. L., Rind, D., Stone, P., Lacis, A. and co-authors. 1983. Efficient three-dimensional models for climatic studies. *Mon. Weather Rev.* **111**, 609–662.

Held, I. M. and Zhao, M. 2011. The response of tropical cyclone statistics to an increase in CO_2 with fixed sea surface temperatures. *J. Clim.* **20**, 5353–5364.

Horn, M., Walsh, K., Zhao, M., Camargo, S. J., Scoccimarro, E. and co-authors. 2014. Tracking scheme dependence of simulate tropical cyclone response to idealized climate simulations. *J. Clim.* **27**, 9197–9213.

Hurley, J. V. and Boos, W. R. 2015. A global climatology of monsoon low pressure systems. *Q. J. Roy. Meteorol. Soc.* **141**, 1049–1064.

JTWC. 2016. *Joint Typhoon Warning Center Tropical Cyclone Best Track Data Site*. Online at: http://www.npmoc.navy.mil

Kim, D., Sobel, A. H., Del Genio, A. D., Chen, Y., Camargo, S. J. and co-authors. 2012. The tropical subseasonal variability simulated in the NASA GISS general circulation model. *J. Clim.* **25**, 4641–4659.

Knutson, T. R., McBride, J., Chan, J., Emanuel, K. A., Holland, G. and co-authors. 2010. Tropical cyclones and climate change. *Nat. Geosci.* **3**, 157–163.

Koch, D., Bayer, S. E., Del Genio, A. D., Faluvegi, G., McConnell, J. R. and co-authors. 2011. Coupled aerosol-chemistry-climate twentieth-century transient model investigation: trends in short-lived species and climate responses. *J. Clim.* **24**, 2693–2714.

Kossin, J. P. and Camargo, S. J. 2009. Hurricane track variability and secular potential intensity trends. *Clim. Change.* **9**, 329–337.

Landman, W. A., Seth, A. and Camargo, S. J. 2005. The effect of regional climate model domain choice on the simulation of tropical cyclone-like vortices in the Southwestern Indian Ocean. *J. Clim.* **18**, 1263–1274.

Landsea, C. W. and Franklin, J. L. 2013. Atlantic hurricane database uncertainty and presentation of a new database format. *Mon. Weather Rev.* **141**, 3576–3592.

Manganello, J. V., Hodges, K. I., Dirtmeyer, B., Kinter, J. L., Cash, B. A. and co-authors. 2014. Future changes in the western North Pacific tropical cyclone activity projected by a multi-decadal simulation with a 16-km global atmospheric GCM. *J. Clim.* **27**, 7622–7646.

Maue, R. N. 2009. Northern hemisphere tropical cyclone activity. *Geophys. Res. Lett.* **36**, L05805.

Maue, R. N. 2011. Recent historically low global tropical cyclone activity. *Geophys. Res. Lett.* **38**, L14803.

Meehl, G., Covey, C., Delworth, T., Latif, M., McAvaney, B. and co-authors. 2007. The WCRP CMIP3 multimodel dataset: a new era in climate change research. *Bull. Am. Meteorol. Soc.* **88**, 1383–1394.

Mei, W., Xie, S.-P. and Zhao, M. 2014. Variability of tropical cyclone track density in the North Atlantic: observations and high-resolution simulations. *J. Clim.* **27**, 4781–4796.

Miller, R. L., Schmidt, G. A., Nazarenko, L. S., Tausnev, N., Bauer, S. E. and co-authors. 2014. CMIP5 historical simulations (1850–2012) with GISS ModelE2. *J. Adv. Model. Earth Syst.* **6**, 441–477.

Murakami, H., Mizuta, R. and Shindo, E. 2012a. Future changes in tropical cyclone activity projected by multi-physics and multi-SST ensemble experiments using the 60-km-mesh MRI-AGCM. *Clim. Dynam.* **39**, 2569–2584.

Murakami, H., Vecchi, G. A., Underwood, S., Delworth, T., Wittenberg, A. T. and co-authors. 2015. Simulation and prediction of category 4 and 5 hurricanes in the high-resolution GFDL HiFLOR coupled climate model. *J. Clim.* **28**, 9058–9079.

Murakami, H., Wang, Y., Yoshimura, H., Mizuta, R., Sugi, M. and co-authors. 2012b. Future changes in tropical cyclone activity projected by the new high-resolution MRI-AGCM. *J. Clim.* **25**, 3237–3260.

Nazarenko, L., Schmidt, G. A., Miller, R. L., Tausnev, N., Kelley, M. and co-authors. 2015. Future climate change under RCP emission scenarios with GISS ModelE2. *J. Adv. Model. Earth Syst.* **7**, 244–267.

Patricola, C. M., Saravanan, R. and Chang, P. 2014. The impact of the El-Niño-Southern Oscillation and Atlantic Meridional Mode on seasonal tropical cyclone activity. *J. Clim.* **27**, 5311–5328.

Reed, K. A., Bacmeister, J. T., Rosenblum, N. A., Wehner, M. F., Bates, S. C. and co-authors. 2015. Impact of the dynamical core on the direct simulation of tropical cyclones in a high-resolution global model. *Geophys. Res. Lett.* **42**, 3603–3608.

Reed, K. A. and Jablonowski, C. 2011. Assessing the uncertainty in tropical cyclone simulations in NCAR's Community Atmosphere Model. *J. Adv. Model. Earth Syst.* **3**, M08002. DOI: http://dx.doi.org/10.1029/2011MS000076

Rind, D., Suozzo, R., Balachandran, N. K., Lacis, A. and Russell, G. 1988. The GISS global climate-middle atmosphere model. Part I: model structure and climatology. *J. Atmos. Sci.* **45**, 329–370.

Roberts, M. J., Vidale, P. L., Mizienlinski, M. S., Demory, M.-E., Schiemann, R. and co-authors. 2015. Tropical cyclones in the UPSCALE ensemble of high-resolution global climate models. *J. Clim.* **28**, 574–596.

Schemm, J.-K. and Long, L. 2013. *Dynamic Hurricane Prediction with the NCEP CFS CGCM. US CLIVAR Hurricane Workshop*. Geophysical Fluid Dynamics Laboratory, Princeton, NJ.

Schmidt, G. A., Kelley, M., Nazarenko, L., Ruedy, R., Russell, G. L. and co-authors. 2014. Configuration and assessment of GISS ModelE2 contributions to the CMIP5 archive. *J. Adv. Model. Earth Syst.* **6**, 141–184.

Schmidt, G. A., Ruedy, R., Hansen, J. E., Aleinov, I., Bell, N. and co-authors. 2006. Present day atmospheric simulations using GISS ModelE: comparison to in-situ, satellite and reanalysis data. *J. Clim.* **19**, 153–192.

Scoccimarro, E., Gualdi, S., Villarini, G., Vecchi, G. A., Zhao, M. and co-authors. 2014. Increased precipitation events associated with landfalling tropical cyclones in response to a warmer climate and increased CO_2. *J. Clim.* **27**, 4642–4654.

Shaevitz, D. A., Camargo, S. J., Sobel, A. H., Jonas, J. A., Kim, D. and co-authors. 2014. Characteristics of tropical cyclones in high-resolution models of the present climate. *J. Adv. Model Earth Syst.* **6**, 1154–1172.

Sherwood, S. C., Ingram, W., Tsushima, Y., Satoh, M., Roberts, M. and co-authors. 2010. Relative humidity changes in a warmer climate. *J. Geophys. Res.* **115**, D09104.

Shindell, D. T., Pechony, O., Voulgarakis, A., Faluvegi, G., Nazarenko, L. and co-authors. 2013. Interactive ozone and methane chemistry in GISS-E2 historical and future climate simulations. *Atmos. Chem. Phys.* **13**, 2653–2689.

Stan, C. 2012. Is cumulus convection the concertmaster of tropical cyclone activity in the Atlantic? *Geophys. Res. Lett.* **39**, L19716.

Strachan, J., Vidale, P. L., Hodges, K., Roberts, M. and Demory, M.-E. 2013. Investigating global tropical cyclone activity with a hierarchy of AGCMs: the role of model resolution. *J. Clim.* **26**, 133–152.

Strazzo, S., Elsner, J. B., LaRow, T. and Halperin, D. J. 2013. Observed versus GCM-generated local tropical cyclone frequency: comparisons using a spatial lattice. *J. Clim.* **26**, 8257–8268.

Suarez, M. J. and Takacs, L. L. 1995. *Documentation of the Aries/Geos Dynamical Core Version 2*. Technical Report Series on Global Modelling and Data Assimilation, NASA Technical Memorandum 104606 Vol. 5, Goddard Space Flight Center, Greenbelt, MD, 58 pp.

Tang, B. and Camargo, S. J. 2014. Environmental control of tropical cyclones in CMIP5: a ventilation perspective. *J. Adv. Model. Earth Syst.* **6**, 115–128.

Tang, B. and Emanuel, K. 2012. A ventilation index for tropical cyclones. *Bull. Am. Meteorol. Soc.* **93**, 1901–1912.

Taylor, K. E., Stouffer, R. J. and Meehl, G. A. 2012. An overview of CMIP5 and the experiment design. *Bull. Am. Meteorol. Soc.* **93**, 485–498.

Tippett, M. K., Camargo, S. J. and Sobel, A. H. 2011. A Poisson regression index for tropical cyclone genesis and the role of large-scale vorticity in genesis. *J. Clim.* **24**, 2335–2357.

Tippett, M. K., Sobel, A. H. and Camargo, S. J. 2012. Association of monthly US tornado occurrence with large-scale atmospheric parameters. *Geophys. Res. Lett.* **39**, L02801.

Tippett, M. K., Sobel, A. H., Camargo, S. J. and Allen, J. T. 2014. An empirical relation between US tornado activity for monthly environmental parameters. *J. Clim.* **27**, 2983–2999.

Vecchi, G. A. and Soden, B. J. 2007. Effect of remote sea surface temperature change on tropical cyclone potential intensity. *Nature*. **450**, 1066–1070.

Villarini, G., Lavers, D. A., Scoccimarro, E., Zhao, M., Wehner, M. F. and co-authors. 2014. Sensitivity of tropical cyclone rainfall to idealized global scale forcings. *J. Clim.* **27**, 4622–4641.

Vitart, F., Anderson, J. L., Sirutis, J. and Tuleya, R. E. 2001. Sensitivity of tropical storms simulated by a general circulation model to cumulus parameterization. *Q. J. R. Meteorol. Soc.* **127**, 25–51.

Vitart, F., Anderson, J. L. and Stern, W. F. 1997. Simulation of interannual variability of tropical storm frequency in an ensemble of GCM integrations. *J. Clim.* **10**, 745–760.

Voulgarakis, A., Telford, P. J., Aghedo, A. M., Braeckside, P., Falugevi, G. and co-authors. 2011. Global multi-year O_3-CO correlation patterns from models and TES satellite observations. *Atmos. Chem. Phys.* **11**, 5819–5838.

Walsh, K., Lavender, S., Murakami, H., Scoccimarro, E., Caron, L.-P. and co-authors. 2010. The tropical cyclone climate model intercomparison. In: *Vol. 2 of Hurricanes and Climate Change* (eds. J. B. Elsner, R. E. Hodges, J. C. Malmstad and K. N. Scheitlin). Springer Verlag, Heidelberg, pp. 1–23.

Walsh, K. J. E., Camargo, S. J., Vecchi, G. A., Daloz, A. S., Elsner, J. and co-authors. 2015. Hurricanes and climate: the US CLIVAR working group on hurricanes. *Bull. Am. Meteorol. Soc.* **96**, 997–1017.

Wang, H., Long, L., Kumar, A., Wang, W., Schemm, J.-K. E. and co-authors. 2014. How well do global climate models simulate the variability of Atlantic tropical cyclones associated with ENSO? *J. Clim.* **27**, 5673–5692.

Wehner, M., Prabhat, M., Reed, K. A., Stone, D., Collins, W. D. and co-authors. 2015. Resolution dependence of future tropical cyclone projections of CAM5.1 in the US CLIVAR hurricane working group idealized configurations. *J. Clim.* **28**, 3905–3925.

Wehner, M. F., Reed, K., Li, F., Prabhat, J., Bacmeister, C. T. and co-authors. 2014. The effect of horizontal resolution on simulation quality in the Community Atmospheric Model, CAM5.1. *J. Adv. Model. Earth Syst.* **6**, 980–997.

Wing, A. A., Sobel, A. H. and Camargo, S. J. 2007. The relationship between the potential and actual intensities of tropical cyclones. *Geophys. Res. Lett.* **34**, L088410.

Wright, J. S., Sobel, A. and Galewsky, J. 2010. Diagnosis of zonal mean relative humidity changes in a warmer climate using tracers of last saturation. *J. Clim.* **23**, 4556–4569.

Yoshimura, J. and Sugi, M. 2005. Tropical cyclone climatology in a high resolution AGCM – impacts of SST warming and CO_2 increase. *SOLA*. **1**, 133–136.

Zhao, M., Held, I. M. and Lin, S.-J. 2012. Some counter-intuitive dependencies of tropical cyclone frequency on parameters in a GCM. *J. Atmos. Sci.* **69**, 2272–2283.

Zhao, M., Held, I. M., Lin, S.-J. and Vecchi, G. A. 2009. Simulations of global hurricane climatology, interannual variability and response to global warming using a 50 km resolution GCM. *J. Clim.* **22**, 6653–6678.

Zhao, M., Held, I. M., Vecchi, G., Scoccimarro, E., Wang, H. and co-authors. 2013. Robust direct effect of increasing atmospheric CO_2 concentration on global tropical cyclone frequency: a multi-model inter-comparison. *US CLIVAR Variations*. **11**(3), 17–24.